ANALYSIS OF ATMOSPHERIC EFFECTS DUE TO ATMOSPHERIC OXYGEN ON A WIDEBAND DIGITAL SIGNAL IN THE 60 GHZ BAND

By
Adelia C. Valdez

Thesis submitted to the Faculty of the
Virginia Polytechnic Institute and State University
(Virginia Tech)
in partial fulfillment of the requirements for the degree of

Master of Science
In
Electrical Engineering

Dr. Timothy Pratt, Chair
Dr. Charles Bostian
Dr. Dennis Sweeney

July 2001
Blacksburg, VA

Keywords: 60 GHz, Wideband Signals, atmospheric absorption, oxygen resonance

AN ANALYSIS OF ATMOSPHERIC EFFECTS DUE TO ATMOSPHERIC OXYGEN ON A WIDEBAND DIGITAL SIGNAL IN THE 60 GHZ BAND

Adelia C. Valdez

Abstract

As lower microwave frequency bands become saturated with users, there is a motivation for the research of applications that utilize higher frequencies, especially the 60 GHz band. This band is plagued with high atmospheric absorption due to atmospheric oxygen, but has a lot of bandwidth, which makes it desirable for multi-media applications. Recently, research of wideband digital links within the 60 GHz band gained the interest of the wireless communication industry when the FCC announced that a license is not required for a wideband digital signal in this band.

Previous research on 60 GHz signals focused on how much attenuation due to atmospheric oxygen exists in the link. But a look at the physical properties of atmospheric oxygen reveals both the reason why atmospheric oxygen absorbs electromagnetic waves and how pressure affects atmospheric oxygen. Atmospheric oxygen resonates at 60 GHz due to transitions between its three closely spaced rotational states. These transitions, combined with the magnetic dipole moment of atmospheric oxygen, cause attenuation and phase dispersion in electromagnetic waves.

At lower pressures, the individual resonance lines of atmospheric oxygen appear in the attenuation and the phase dispersion plots. As pressure increases, the resonance lines broaden and contribute to neighboring resonant lines. The effect of attenuation and phase dispersion in a wideband signal becomes greater at lower atmospheric pressures, which results in signal distortion. The signal distortion leads to more bit errors and results in the presence of inter-symbol interference (ISI) in the received signal.

This thesis aims to analyze the effects of atmospheric oxygen on a wideband digital link, especially at lower pressures and higher data rates. In order to simulate the effects of atmospheric oxygen in the atmosphere, an empirical atmospheric model was used, which characterizes the behavior of oxygen under various atmospheric pressures. A wideband

communication system was simulated with the absorption and dispersion due to atmospheric oxygen represented as a transfer function and placed in the link part of the system. Eye diagrams were used to view the impact of the atmospheric oxygen attenuation and phase dispersion in the signal. Also bit error rate plots were computed in order to determine the extra margin needed.

Acknowledgments

I want to begin by thanking my advisor and committee chair, Dr. Pratt, who suggested the topic for this thesis. He always had suggestions for my simulations, answered my numerous questions, and put forth the effort to make sure I finished my thesis before leaving Blacksburg. I offer my gratitude to Dr. Bostian and Dr. Sweeney for serving on my committee and for reading this thesis within a short time frame.

I want to thank my family for always supporting my strive for more and never settling for less. I offer my appreciation to Yonatan Fridman for his help, encouragement, and support throughout the duration of this thesis.

Table of Contents

List of Figures

List of Tables

Chapter 1 - Introduction

Previously the band of 50 to 70 GHz was avoided because of the high attenuation of signal strength due to atmospheric oxygen. Today, research is in progress for digital wireless applications in the 60 GHz band. Current wireless applications include inter-satellite links, collision warning systems, road monitoring systems, railroad communication systems, and military field applications. A few advantages of using the 60 GHz band include unlicensed operation in the US, wide bandwidths, and the presence of high attenuation, which aids in minimizing the interference between neighboring cellular channels, and helps in preventing unauthorized users from intercepting a transmission.

The major difficulties for a signal in the 60 GHz band are atmospheric absorption and phase dispersion by oxygen, water vapor, and raindrops. Due to its magnetic dipole moment, the oxygen molecule absorbs power and causes phase dispersion of an electromagnetic wave between the frequencies of 50 GHz and 70 GHz. Although attenuation due to atmospheric oxygen at sea level is around 15 dB/km, experts in industry are utilizing the attenuation to minimize interference between channels. However, with wideband digital signals, phase dispersion may cause parts of a digital waveform to fall into neighboring time slots (either the previous bit or the next bit), causing inter-symbol interference (ISI).

The aim of this research is to determine how the atmospheric oxygen molecule causes attenuation, phase dispersion, and group delay in the link, as well as how it affects a wideband digital signal. The physics of the oxygen molecule was studied in order to comprehend its complex molecular behavior, such as pressure broadening and appearance of several resonance frequency lines. An empirical atmospheric model was used to simulate the behavior of oxygen under various atmospheric pressures, where the behavior of oxygen was modeled as a transfer function. An eye diagram was used to visualize the effects of atmospheric oxygen on a wideband digital signal, such as introducing ISI into the signal.

1.1 Problem Overview

The complex physics of the O_2 molecule must first be understood in order to determine how atmospheric oxygen attenuation affects a wideband digital system operating at 60 GHz. Essentially, the magnetic dipole moment combined with the resonance of atmospheric oxygen molecule causes the molecule to absorb electromagnetic waves around 60 GHz.

The behavior of atmospheric oxygen is frequency and pressure dependent. At lower atmospheric pressures, individual resonance lines are visible in the attenuation and phase dispersion curves, as seen in Figure 1.1 and Figure 1.2. As the pressure increases, the width of individual resonance lines increases and contributes to neighboring line frequencies, leading to a higher total attenuation centered about 60 GHz. Figure 1.1 displays the specific attenuation of atmospheric oxygen with a pressure of 75 mbar, and Figure 1.3 displays the specific attenuation of atmospheric oxygen for a pressure of 1013 mbar. These plots were generated using an empirical model for atmospheric oxygen developed by Hans J. Liebe [1]. In Figure 1.1, the peak atmospheric oxygen attenuation is almost 6 dB/km, and the individual lines are noticeable and spaced less than 1 GHz apart. With an increase in pressure, the individual lines broaden and blend together, creating the smooth plot shown in Figure 1.3. As a result of the individual line contributions, the attenuation in Figure 1.3 is 16 dB/km. An atmospheric pressure of 1013 mbar corresponds to sea level, and 75 mbar corresponds to an altitude of 18 km (59,400 ft), based on a standard atmosphere.

Figure 1.2 and Figure 1.4 show the phase dispersion and group delay due to atmospheric oxygen at 75 mbar and 1013 mbar, respectively. The individual resonance lines are also visible in the phase dispersion and group delay at 75 mbar. In Figure 1.2 and in Figure 1.4, changes in phase and in time exist in the phase dispersion and group delay plots, respectively. These rapid changes mostly likely introduce ISI in digital links, but the effect of this interference is unknown.

After understanding the physics of the atmospheric oxygen molecule, a search for an atmospheric model was conducted. Slant path propagation textbooks cover atmospheric attenuation except for a few frequencies, especially between 50 GHz and 70 GHz [2]. Instead, a complex model developed by Liebe was used to simulate atmospheric conditions for dry air. Once the model was understood and was simulated properly, the next issue at hand was how to implement the nonlinear amplitude and phase transfer functions of the model into the system, and how to modify the model for conditions simulated in this research. The model developed by

Liebe, which is referred to as Liebe's model or atmospheric model in this thesis, was programmed into MATLAB, where the data and plots were obtained.

After simulating the atmospheric model, it was replicated in a simple BPSK system. Along with implementing the model, a simple eye diagram and bit error rate (BER) plots were generated in order to determine if the atmospheric oxygen had introduced ISI into the link and to determine the additional margin needed to meet the required carrier to noise ratio (C/N).

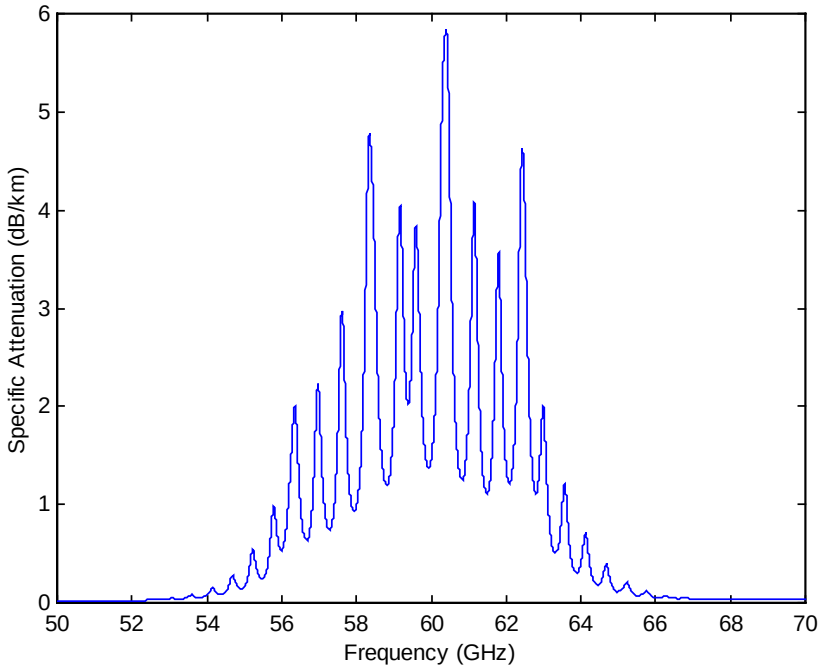

Figure 1.1 - Specific attenuation of atmospheric oxygen at a pressure of 75 mbar and an altitude of 18 km (59,400 ft) based on a standard atmosphere.

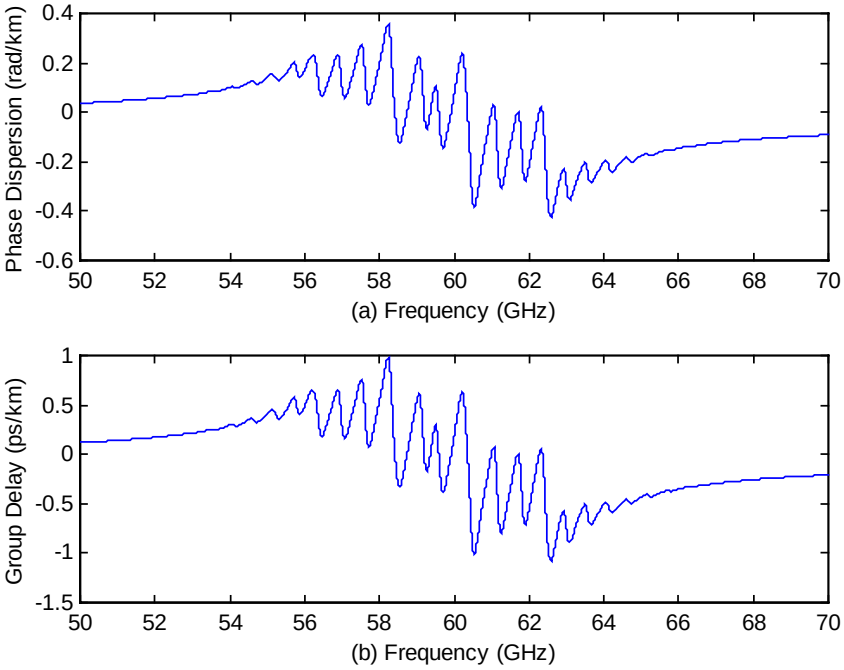

Figure 1.2 - Phase dispersion (a) and group delay (b) of atmospheric oxygen at $P = 75$ mbar.

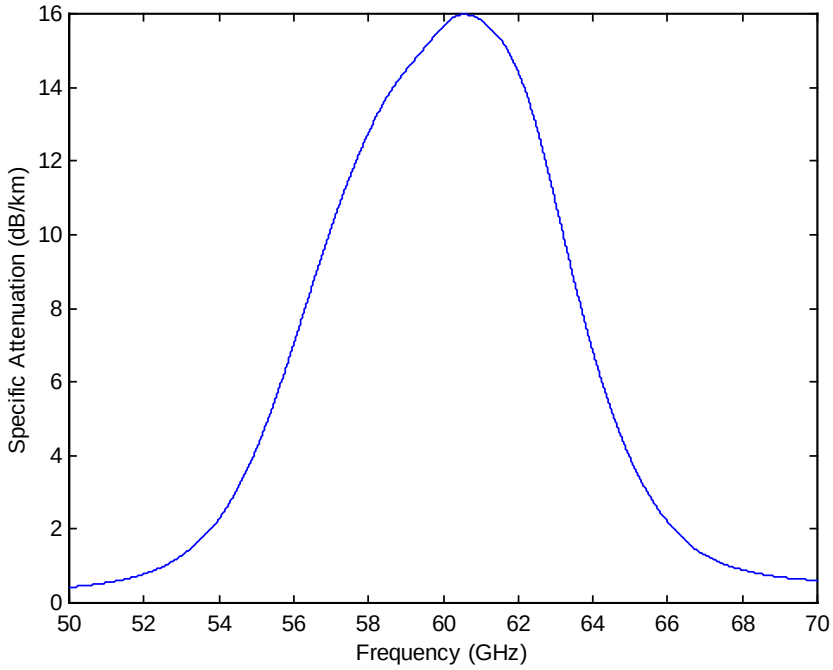

Figure 1.3 - Specific attenuation of atmospheric oxygen at a pressure of 1013 mbar found at sea level based on a standard atmosphere.

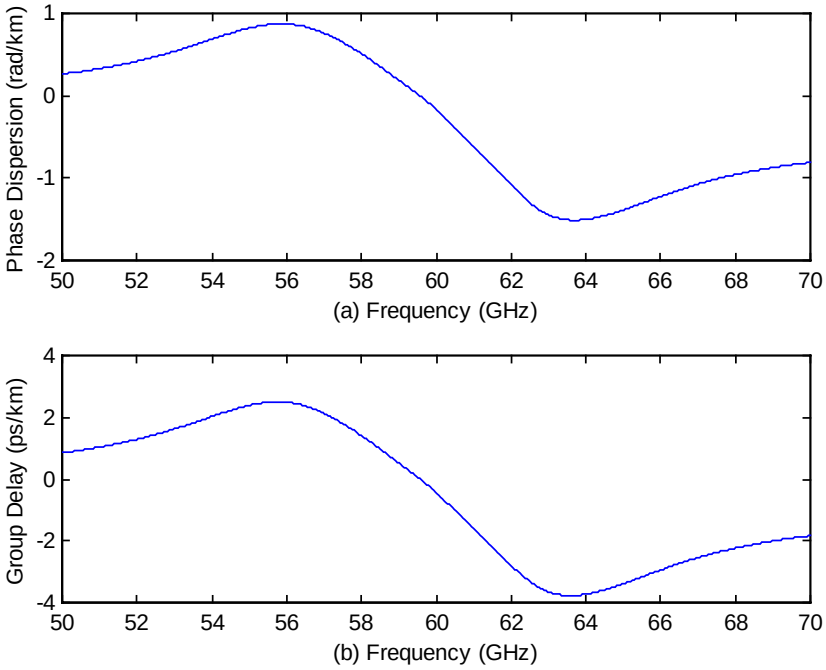

Figure 1.4 - Phase dispersion (a) and group delay (b) of atmospheric oxygen at P = 1013 mbar.

1.2 Problem Significance

Most of the research concerning signals in the 60 GHz band discusses how much attenuation due to atmospheric oxygen exists and how it is useful for minimizing interference, but fails to mention the impact of phase dispersion and group delay due to the oxygen. For communication systems with low data rates, the presence of phase dispersion and group delay due to atmospheric oxygen has little effect on the signal. But as the data rate increases phase dispersion and group delay cause distortion and introduce ISI in the received wideband digital signal.

In 1996, the FCC announced that a license is not required for a wideband digital signal in the 60 GHz band (59 – 64 GHz) [3], [4]. With this announcement, wireless companies were motivated to develop wireless fiber radio systems, where the radio provides a virtual or wireless link between two fibers. The main objective for these radios is to eliminate the "last mile" costs. The manufacturers are claiming that the fiber radios are capable of full-duplex communication using a data rate of 1 Gbps. The fiber radios are discussed further in Section 1.3.8.

At sea level, the phase dispersion due to atmospheric oxygen introduces a small amount of distortion into the signal, which is accounted for by including a small margin in the link budget. As the atmospheric pressure becomes smaller, individual resonance lines of the oxygen molecule appear, causing more phase distortion in the signal. In order to compensate for this phase distortion, the link budget needs more than a small margin to achieve a desired BER at a specific carrier to noise ratio (C/N).

1.3 Wireless Applications for Operation in the 60 GHz Band

Utilizing the frequencies between 50 GHz and 70 GHz was traditionally avoided but now applications are being developed. The need for larger bandwidth, which is available with higher frequencies, motivates the research of cellular scenarios. Other applications are developed out of necessity to keep communication signals from undesired listeners. Currently, exploration of the 60 GHz band covers the following areas [5]:

- Broadband Networks and Services
- Indoor and Cordless Phones
- Road Transport Informatics Systems
- Railway Communications
- Aircraft Communications
- Inter-Satellite Links
- Military Communications
- Other Applications

The scenarios discussed in this section originate from a survey of wireless applications in the 60 GHz band [5]. The majority of the applications discussed in the following sections stem from research conducted by different European organizations and utilize low data rates. A few broadband applications are also presented.

1.3.1 Broadband Networks and Services

The wide bandwidth in the 60 GHz band is appealing for providing high-speed video and/or data transmission to fixed and/or mobile users [5], [6]. Currently, the European Union (EU) funds two projects, RACE 2 and ACTS. The main objective of these projects is to analyze the feasibility and implementation of broadband networks.

A team of European partners developed Mobile Broadband System (MBS), which is a sub project of RACE 2. The mission for MBS involves researching the feasibility of a 60 GHz radio link with the capabilities of transmitting up to 32 Mbps from a vehicle to a fixed beacon and up to 155 Mbps in a cellular environment [7], [8]. The MBS intends to utilize the research conducted for the development of RF, IF, and baseband systems capable of operating with a high data rate in the 60 GHz band.

The sub project MEDIAN was developed to pursue the implementation of a high-speed wireless local area network (WLAN) for multimedia, voice, and video applications and is currently active within the ACTS project [9]. This system utilizes Orthogonal Frequency-Division Multiplexing (OFDM), supports Asynchronous Transfer Mode (ATM), and provides bit rates up to 155 Mbps. As part of an ACTS project, MEDIAN plans to integrate the fixed B-ISDN services by using local wireless broadband transmission and data interfacing to the fixed ATM network for single and multiple base stations sited in a local area.

Another ACTS project pursuing development of 60 GHz systems is the SAMBA project [10]. The goal of SAMBA is to extend broadband connectivity to mobile users through the development of a wireless network that provides multimedia and high-speed services through transparent ATM links. The systems developed support data rates up to 34 Mbps and are useful for such applications as database information access, transmission of medical images, wireless TV cameras, etc.

1.3.2 Indoor and Cordless Phones

Microcellular structures operating at 60 GHz are useful for indoor applications, such as within large corporate or government office buildings, where large bandwidths are suited for high transmission within a crowded environment [5], [11]. The advantages of using an indoor phone system are increased capacity, simpler network management (cable laying and maintenance is minimized), flexibility in the allocation of new users, and terminal mobility. On the other hand, this system is susceptible to a reduction in signal strength due to the material used to construct the building and partitioning within the building, and severe multipath propagation can occur due to reflections from internal surfaces [12], [13], [14].

1.3.3 Road Transport Informatics Systems

Uses for millimeter waves exist in vehicle-vehicle and vehicle-fixed base station communication applications [5]. These radio links are concentrated on roads and highways in open sub-urban/rural areas with few or no surrounding buildings [15]. The cell shape provides coverage strictly to users on the road, which is possible based on the antenna radiation patterns. Clusters of cells are arranged in a linear pattern, instead of the traditional hexagonal cell pattern. Researchers discovered that microcells spanning 90 m along highway lanes supported a system with 1562 BPSK-modulated channels, where each channel had a bandwidth of 40 kHz, a bit rate of 32 kb/s, and a C/I of 26 dB.

PROMETHEUS is a EU project aimed at improving the efficiency/safety of road transportation in Europe. The main issues addressed by this project are automated traffic management, drive assistance and integration between vehicles and traffic control, and enhanced safety for travelers [16]. In order to meet these requirements, researchers of the PROMETHEUS project developed advanced electronic, computer, and telecommunication technologies capable of 1) exchanging information between vehicles and between vehicles and fixed base stations and 2) monitoring real-time traffic control.

One project within PROMETHEUS, COPDRIVE, developed a system aimed at reducing the risk of road accidents and traffic jams. The system architecture consists of radio equipment with vehicle-to-vehicle and vehicle-to-infrastructure communication capabilities, and precision sensors that measure the relative positions of nearby vehicles. On-board software organizes the radio equipment and sensors and manages cooperative driving strategies [17].

Within this system, each vehicle continuously exchanges information with the roadside base stations and nearby vehicles. For example, the vehicle relays the current weather conditions to the base station and other vehicles. If drivers turn on their fog lights, the vehicle notifies the base station that fog exists on this particular stretch of road. Also vehicles are informed if a collision exists on a highway or road. When a crash transmitter is activated due to the occurrence of a collision, the computer on-board the vehicle notifies nearby vehicles and base stations about the location of the collision. Base stations also convey information about current traffic and weather conditions, recommended driving speed, etc. to vehicles and other base stations.

The communication systems onboard vehicles operate at 60 GHz, where obstructions attenuate the signal, in some cases even more than the attenuation due to atmospheric oxygen. Table 1.1 lists the obstructions that attenuate a signal while on the road [5], [17], [18]. At short distances a bicycle, motorcycle, and pedestrian obstruct or attenuate the signal transmitted from the vehicle by less than 10 dB. Larger obstructions, such as a nearby bus, car, truck, or tree branches, attenuate the same signal by 10 dB or more.

Table 1.1 - Attenuation of Signal Strength due to Obstructions at 60 GHz [5]

Obstruction	*Attenuation*
Pedestrian	7-8 dB
Tree branches	10 dB
Vehicles	10-14 dB
Bicycle and Motorcycle	4 dB
Trucks and Buses	15-33 dB

1.3.4 Railway Communications

Modern railway systems need an efficient communication system between the control center and other trains [19]. Such a communication system requires low to medium data rates for handling traffic control information and minimal reciprocal interference with other communication systems. The Germany Federal Railways Company (DBB) experimented with a communication system that uses ASK modulation, operating at 35 and 58 GHz with a data rate of 64 kbps [20]. Radio coverage of the railway line consists of adjacent rectangular cells lined up in a row to match the shape of the railway. In preliminary tests, researchers discovered that the communication system operating at 35 GHz was susceptible to strong multipath propagation and that the tunnels appeared as large waveguides. At 58 GHz, multipath propagation and waveguide effects inside the tunnels were considerably reduced because of atmospheric oxygen attenuation.

1.3.5 Aircraft Communications

Aircraft passengers are prohibited from using their cell phones, which operate in the UHF (900 MHz or 2 GHz) bands, on flights because of the potential for interference with avionics instrumentation [21]. A proposed solution [22] to this problem is to use the 60 GHz band for aircraft-satellite communications. The European Space Agency (ESA) carried out a study [23] to determine possible communication scenarios for providing service to aircraft passengers. In one scenario, the aircraft is viewed as a single cell with its own base station that sends calls originated by airline passengers to a geostationary (GEO) satellite, which acts as a repeater and relays the calls to a ground station. For this scenario, the use of the 60 GHz band is restricted to the aircraft-satellite link only, as seen in Figure 1.5. The aircraft needs to be visible to the satellite during the entire flight. Preliminary link budget results were rather discouraging, since transmission from the aircraft to the satellite requires high RF power when the aircraft can only accommodate a moderately sized antenna. Figure 1.5 represents the envisioned aircraft to satellite link. The downlink from the satellite to the ground station in Figure 1.5 is unknown from [5].

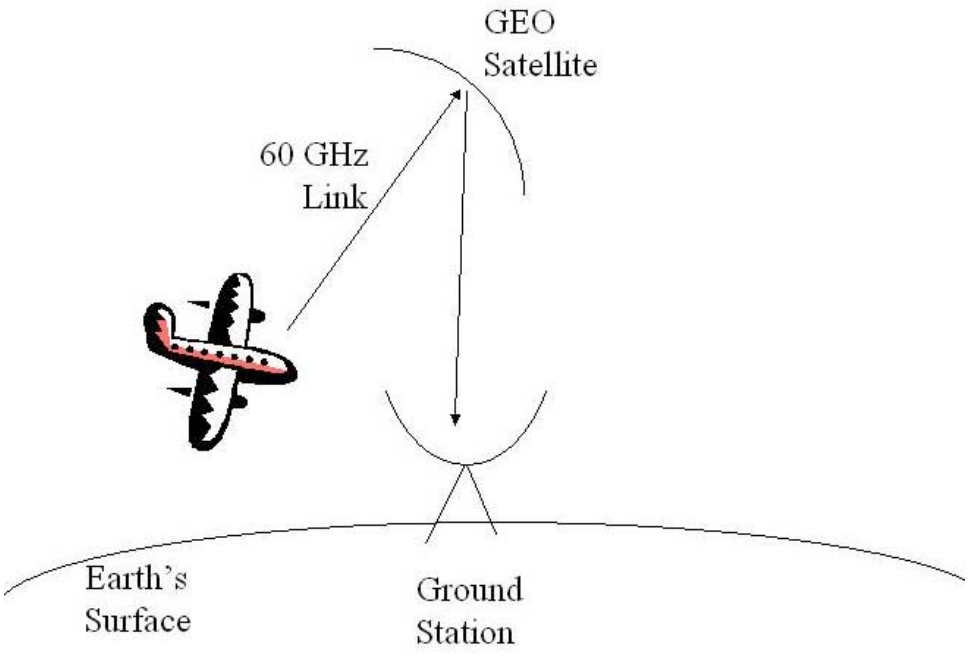

Figure 1.5 - Aircraft to satellite multi-channel phone link.

1.3.6 Inter-Satellite Links

In the early 1980s, ESA [23] and NASA [24] investigated the application of the 60 GHz band for inter-satellite communication links. In this scenario, signals are subject only to free-space loss, since the radio path lies totally outside the atmosphere and the atmospheric oxygen belt surrounding the Earth prevents interference from and to ground stations. ESA proposed an inter-satellite link between two GEO satellites spaced 50 degrees apart with a high-gain antenna (55 dBi), a data rate of 120 Mbps, and transmit power of less than 8 W. NASA envisioned the use of two (or more) GEO satellites to relay signals between two earth stations that were too distant to be linked by one satellite. Their satellites support a throughput of 270 Mbps, transmit power of 100 W, and have 55 dBi antennas. In this same document, NASA also proposed two 60 GHz inter-satellite cross-link applications: 1) communication between satellites arranged in a cluster (spaced less than 50 km apart) and 2) communication between a relay satellite and an orbiting space station.

1.3.7 Military Communications

Radio communication in the 60 GHz band appeals to the military since the link ensures low probability of intercept (LPI) [25] and provides better protection against undesired unauthorized listeners than communication in the HF, VHF, or UHF band. One prototype developed by AEG, Ulm, Germany, is a 60 GHz "walkie-talkie" that has a secure short-range (less than 1.5 km) communications link and has a transmit power of 8 mW [25]. Another prototype developed by Marconi, Stanmore, UK, was the "binocular radio," which has a range of 1 km and has a directive antenna for short-range line of sight (LOS) links that is aimed at the receiver manually through the aid of optical binoculars [26].

1.3.8 Other Applications

In 1996, the FCC and other regulatory bodies approved high data rate, unlicensed wireless communications in the range of 59-64 GHz [3]. The high data rate and unlicensed band of 59-64 GHz attracted companies, leading to the development of broadband LOS and fiber radio systems [27]. One radio system on the market is GigaLink, a fiber radio designed by Harmonix Corporation [28]. The radio is capable of transmitting up to 622 Mbps and utilizes a compact antenna with a focused beam. Features of this system include working in conjunction with

existing fiber, solving the "last mile" challenge, and being an affordable alternative to the expensive and lengthy process of installing fiber [29].

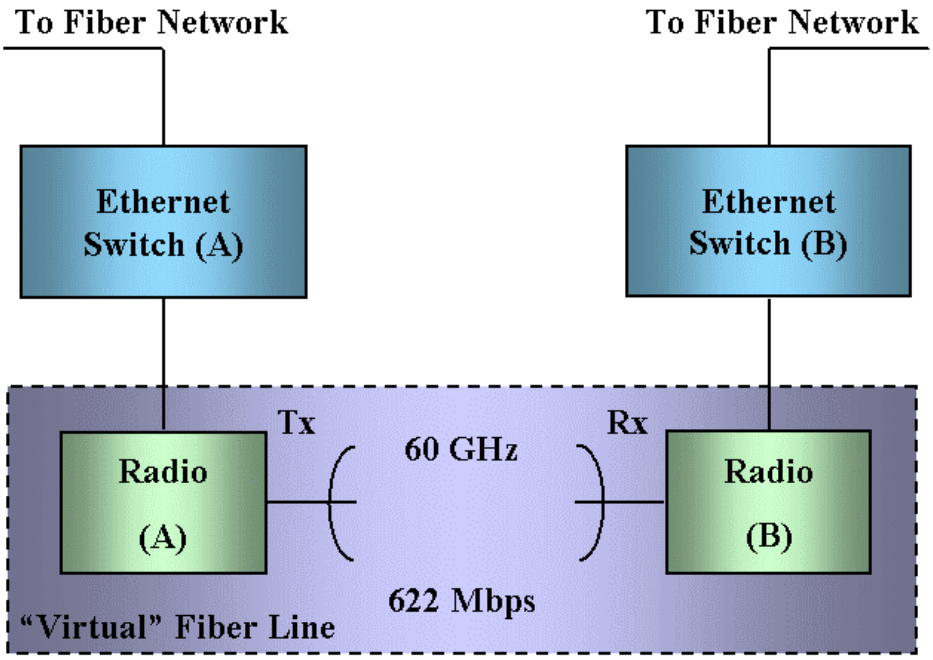

Figure 1.6 - Fiber radio system

Figure 1.6 presents a simple block diagram for a fiber radio system. The radios (radio (A) and radio (B)) appear transparent between Ethernet switches, which connect to the fiber. The Ethernet switches are relays that interact between the information coming from the network and the information passed on to the radio. The dashed box around the two radios represents a "virtual" fiber line between the switches. The information is passed on from the Ethernet switch (A), transmitted by radio (A), received by radio (B) and passed on by Ethernet switch (B) to the fiber network. The fiber network has data rates up to 1 Gbps. The Ethernet switch modifies the information to fit into data rates of 622 Mbps and then reassembles the information to have a gigabit data rate at the receive end.

1.4 Thesis Outline

The theoretical and experimental research is presented in the following chapters. Chapter 2 presents the physics of the oxygen molecule and explains why the molecule absorbs microwaves. The discussion on the spectral line broadening and the behavior of oxygen under atmospheric pressures under different atmospheric pressures is presented in Chapter 2. In order

to model the behavior of atmospheric oxygen, Liebe's empirical model was used, which includes the details for parameters and equations used in the model and is discussed in Chapter 3. Only the dry air analysis of the model is considered in this thesis. The equations for atmospheric attenuation, phase dispersion, and group delay due to atmospheric oxygen are also presented.

The simulation and results are discussed in Chapter 4 and Chapter 5, respectively. Chapter 4 includes simulation parameters, conditions, and equations. The set-up for the eye diagram is also mentioned. Chapter 5 covers the results obtained from the simulations. The results consist of plots and data for a system where the parameters – pressure, data rate, and distance – are varied. Further research possibilities are included in the Conclusion.

Chapter 2 - Background

In the 1940s, physicists studied the properties of the oxygen molecule to determine how and why it absorbs electromagnetic waves in the presence of an atmosphere. They also wanted to understand how individual resonance lines are distinguishable at low pressure but disappear as atmospheric pressure increases. In this chapter, the background for the physical properties of oxygen, the equations for the shape of the attenuation curve, and the behavior of oxygen in the presence of changing air pressure are described.

2.1 Physical Properties of Oxygen

J. H. Van Vleck detailed the physics of atmospheric oxygen absorption at □ = 5 mm in a paper published in 1947 [30], where he presented the background for why atmospheric oxygen absorbs microwaves and resonates in the vicinity of 60 GHz. Atmospheric oxygen is electrically non-polar. Most electrically non-polar molecules absorb electromagnetic waves when electrons transition between two electronic states, causing resonance to occur in the ultraviolet region. Electrically polar molecules absorb electromagnetic waves when transitions between two electrons occur in a single electronic state. Although oxygen is electrically non-polar, it absorbs electromagnetic waves close to □ = 5 mm when transitions occur between closely spaced electrons within a single electronic state.

Oxygen is paramagnetic, which means it has a permanent magnetic dipole moment. Generally, only molecules with electric dipoles were thought to absorb electromagnetic waves. Since Maxwell's equations are symmetric in both the E and H fields, molecules with magnetic dipoles can also absorb waves. Molecules with electric dipoles tend to have a stronger effect on the absorption of electromagnetic waves than their magnetic counterparts. However, with the oxygen molecule, the magnetic absorption has a stronger effect on electromagnetic waves

propagating through the atmosphere if the transmitting frequency is near the resonating frequency of 60 GHz.

When an electromagnetic wave collides with an oxygen molecule, electrons transition within a single electron state, which results in the molecule resonating. As the electron jumps around with a single state, the energy of the electron varies. This change in energy results in frequency of absorption and is represented by

$$\nu_{i,j} = \frac{E_i - E_j}{h} \qquad (1)$$

where $\nu_{i,j}$ is the frequency of absorption, E_i and E_j is the energy of the electron before and after it moved, respectively, and h is the Planck constant. These transitions combined with the magnetic dipole moment of oxygen cause the oxygen molecule to absorb electromagnetic waves in the presence of the atmosphere.

2.2 Atmospheric Oxygen Absorption

In the following sections, the background for the equations developed in Liebe's model is presented. Although these equations are archaic (not in SI units), they provide the reader with an introduction to the equations discussed in Chapter 3.

2.2.1 Atmospheric Oxygen Absorption Formula

Van Vleck proposed equations for calculating the attenuation due to atmospheric oxygen around 60 GHz based on a standard attenuation equation. He first presented the general absorption formula for the specific attenuation, γ, in dB/km [30]

$$\gamma = 10^6 \left(\log_{10} e\right)\left(\frac{8\pi^3 \nu N}{3hc}\right)\frac{\sum_{i,j}\left\{\left|\mu_{i,j}\right|^2 f\left(\nu_{ij},\nu\right)\right\}e^{-E_i/kT}}{\sum_j e^{-E_i/kT}} \qquad (2)$$

where N is the number of molecules per cc; $\mu_{i,j}$ is the matrix element of the dipole moment connecting two stationary states i, j, with energy E_i, E_j; ν_{ij} is the frequency corresponding to the resonant line or absorption; ν is the frequency of the incident radiation; k is Boltzmann constant; h is Planck's constant; and T is the temperature. The $10^6 \log_{10} e$ term allows γ to be expressed in decibels per kilometer, where e = 2.718. Van Vleck's term $f(\nu_{ij}, \nu)$, the structure factor, governs the shape of the absorption line and is expressed by the following unitless function:

$$f(\nu_{ij},\nu)=\frac{\nu}{\pi\nu_{ij}}\left[\frac{\Delta\nu}{(\nu_{ij}-\nu)^2+\Delta\nu^2}+\frac{\Delta\nu}{(\nu_{ij}+\nu)^2+\Delta\nu^2}\right] \quad (3)$$

where □□ is the line-breadth constant or the width of the resonating frequency line. The function $f(\square_{ij}, \square)$ is the early form of the line shape function discussed in 3.2.2.1 and determines the shape of resonating lines in the attenuation curve.

Equation (2) is the foundation for the atmospheric oxygen absorption formula (5). In this absorption formula (5), the indices *i*, *j* in equation (2) are now represented by a trio of quantum numbers *J*, *K*, *S*, which describe the rotational orientation of the oxygen molecule. *K* is orbital momentum. For oxygen, the Pauli exclusion principle allows only odd values of *K*. Pauli's principle says that no state exists in any quantized system in which two electrons are in the same quantum state [31]. *J* is total angular momentum and is defined by

$$J = K + S \quad (4)$$

where *S* is the molecular spin and is also known as the spin quantum number. For oxygen, $S = 1$, then the three quantum states of *J* are *K*-1, *K*, and *K*+1, which are separated by intervals of *K*. The structure of oxygen is classified as a rho-type triplet because the quantum number *J* has three defined states and the individual states, *K*-1, *K*, and *K*+1, are so small they cause resonance to occur at microwave frequencies.

The attenuation formula for atmospheric oxygen involves the rotational behavior of atmospheric oxygen, which is characterized by the quantum numbers *J* and *K*, and is represented by

$$\gamma = 10^6(\log_{10}e)\left(\frac{4\pi^3\nu N}{3ckT}\right)\frac{\sum_K\left\{2\left|\nu_{K+}f(\nu_{K+},\nu)\right|^2\mu_{K+}{}^2+2\left|\nu_{K-}f(\nu_{K-},\nu)\right|^2\mu_{K-}{}^2+F(\nu)\mu_{K_0}{}^2\right\}e^{-E_{Ki}/kT}}{\sum_K 3(2K+1)e^{-E_K/kT}} \quad (5)$$

where $\square_{K+}$ and $\square_{K-}$ represent the center frequency of the spectral line that corresponds to a particular *K* state[1]. The first two terms of the summation in the numerator of □ represent the resonant absorption of atmospheric oxygen, while the third term represents the non-resonant absorption, which is explained in Section 3.2.2.2. The shape function $f(\square_{ij}, \square)$ now includes $\square_{K+}$ and $\square_{K-}$, which produces the following formulas:

[1] The values for $\square_{K+}$ and $\square_{K-}$ are defined in a table listed in [30].

$$f(\nu_{K+},\nu)=\frac{\nu}{\pi\nu_{K+}}\left[\frac{\Delta\nu}{(\nu_{K+}-\nu)^2+\Delta\nu^2}+\frac{\Delta\nu}{(\nu_{K+}+\nu)^2+\Delta\nu^2}\right] \quad (6)$$

and

$$f(\nu_{K-},\nu)=\frac{\nu}{\pi\nu_{K-}}\left[\frac{\Delta\nu}{(\nu_{K-}-\nu)^2+\Delta\nu^2}+\frac{\Delta\nu}{(\nu_{K-}+\nu)^2+\Delta\nu^2}\right] \quad (7)$$

The parameters $F(\square)$, $\square_{K+}{}^2$, $\square_{K-}{}^2$, and $\square_{K0}{}^2$ are expressed as

$$F(\nu)=\frac{2\nu\Delta\nu}{\pi\left(\nu^2+\Delta\nu^2\right)} \quad (8)$$

$$\mu_{K+}{}^2=\frac{4\beta^2K(2K+3)}{K+1} \quad (9)$$

$$\mu_{K-}{}^2=\frac{4\beta^2(K+1)(2K-1)}{K} \quad (10)$$

and

$$\mu_{K0}{}^2=\frac{8\beta^2\left(K^2+K+1\right)(2K+1)}{K(K+1)} \quad (11)$$

The parameter $F(\square)$ characterizes the line shape function for the nonresonant part of the atmospheric oxygen attenuation. The parameters $\square_{K+}{}^2$, $\square_{K-}{}^2$, and $\square_{K0}{}^2$ represent the strength or the intensity of the resonant line. The oxygen molecule carries a magnetic dipole moment with two Bohr magnetons, which are accounted for in the parameters $\square_{K+}{}^2$, $\square_{K-}{}^2$, and $\square_{K0}{}^2$. The Bohr magneton $\square$ is defined as

$$\beta=\frac{he}{4\pi mc} \quad (12)$$

where m is the mass of an electron.

Van Vleck plotted the atmospheric oxygen absorption, which is seen in Figure 2.1. Figure 2.1 displays the theoretical calculation of the atmospheric oxygen attenuation, $\square$, equation (5), where the absorption occurs in dry air with temperature T = 300 K and atmospheric pressure P = 1013 mbar. The atmospheric oxygen absorption is a function of frequency $\square$ in GHz and the attenuation is plotted in dB/km. Rather than plot Figure 2.1 at various pressures, Van Vleck plots the attenuation for various resonance line widths. The short-dashed curve (curve with the lowest peak) represents the attenuation for $\square\square$ = 3 GHz, and the long-dashed curve (the curve with the middle peak) represents $\square\square$ = 1.5 GHz, where $\square\square$ is the

width of each resonance line. The solid curve represents the width of □□ = 0.6 GHz. In this solid curve, the individual resonance lines are visible, whereas in the dashed curves, the width of the resonant line is so broad that the lines overlap each other and merge together.

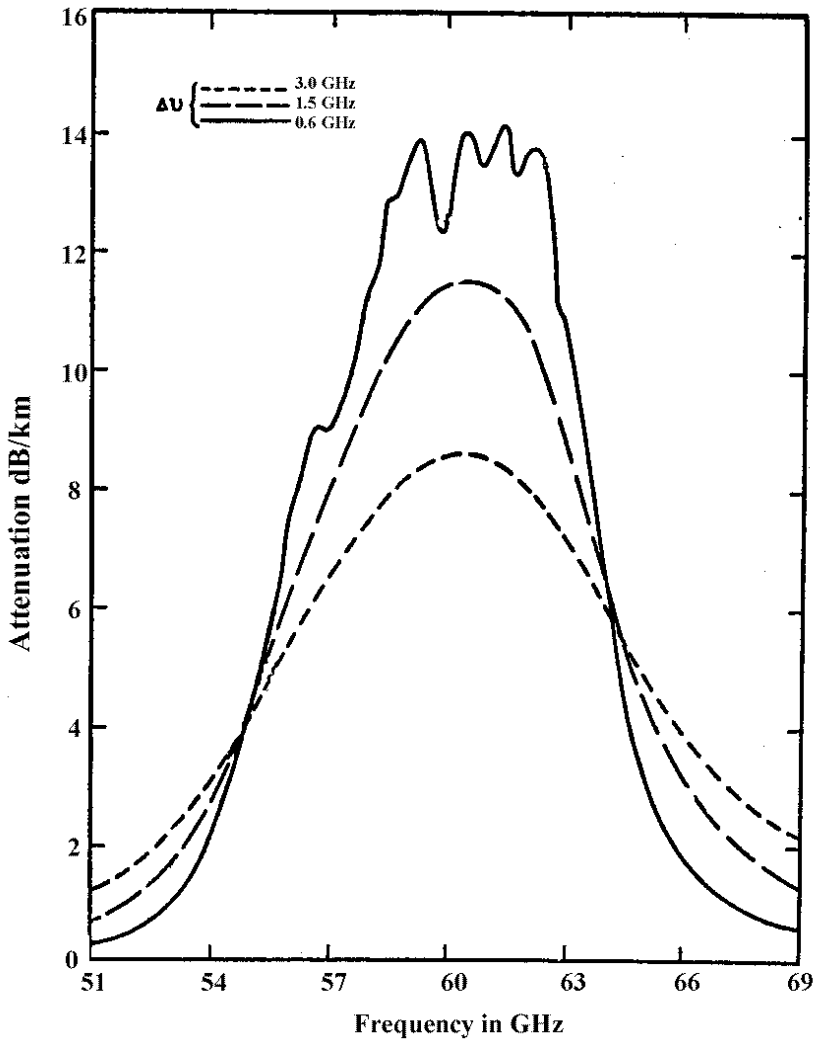

Figure 2.1 - The atmospheric oxygen absorption, □, of dry air at *P* = 1013 mbar for resonance line widths, □□, of 0.6 GHz, 1.5 GHz, and 3.0 GHz [30].

2.2.2 Non-Resonant Part of the Absorption

The third term in equation (5) represents the non-resonant part of atmospheric oxygen absorption [30]. The non-resonant term arises from spectral lines whose resonance frequency is zero. These lines result from the matrix for the spin magnetic moment, which contains non-diagonal and diagonal matrix elements. The non-diagonal elements are responsible for resonance at □ = 5 mm, while the diagonal elements have a resonance frequency that is zero. The non-diagonal and the diagonal matrix elements are produced by the perpendicular and the parallel projections, respectively, of the spin vector ***S*** onto the resultant angular moment vector ***J***. This third term is constant. Normally, one thinks of absorption arising from a variable moment, not a constant moment. But this constant moment is disrupted by molecules colliding and has a radiative effect as a result of molecules trying to realign.

2.3 Spectral Line Broadening

The top line plotted in Figure 2.1 shows individual peaks, which correspond to the resonance of individual frequencies, whereas the two lower plots appear smooth and the location of individual resonance lines is not visible. The appearance of a smooth broad curve is due to frequencies spreading or broadening across other frequencies, which is the result of pressure broadening. Pressure or collision broadening is due to interactions between randomly absorbing gas molecules and is directly related to pressure [32]. As the pressure increases, the lines blend together creating a smooth shape, like the bottom line in Figure 2.1, where the individual resonance lines spread up to about 3 GHz [33].

The concentration of molecules in the atmosphere is directly related to pressure. At higher atmospheric pressure, the concentration of oxygen molecules is high. Electromagnetic waves propagating through the atmosphere at a frequency close to 60 GHz collide with oxygen molecules. These collisions cause the electrons in the molecule to move around within a single electronic state, which cause the molecule to resonate and absorb electromagnetic waves. In order to obey the law of energy conservation, the oxygen molecule also emits energy. This emitted energy along with the energy from the electromagnetic wave are absorbed by neighboring molecules, which is seen in Figure 2.2.

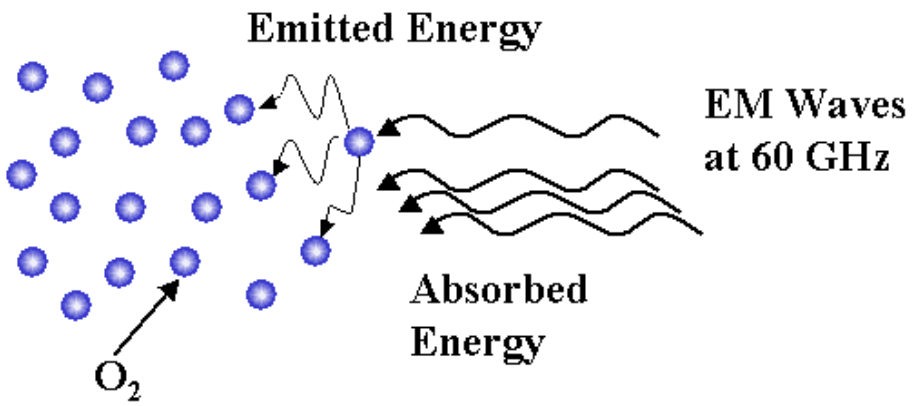

Figure 2.2 – Electromagnetic waves colliding with the oxygen molecule.

The oxygen molecule resonates at frequencies between 50 GHz and 70 GHz. The high concentration of molecules leads to a high rate of collisions between the oxygen molecule and the electromagnetic wave. Each collision results in a resonance frequency when energy is absorbed. Due to the high concentration of collisions, these individual resonance frequencies are not distinguishable. Instead, the width of the lines overlaps and cause higher total attenuation. An attenuation plot for atmospheric oxygen appears broad and smooth.

At lower pressures, there is a smaller concentration of oxygen molecules, leading to fewer collisions between the molecule and an electromagnetic wave. With the occurrence of fewer collisions, individual resonance frequencies are distinguishable and result in a smaller total attenuation due to atmospheric oxygen.

The other three sources of spectral line broadening worth mentioning are natural line width, Doppler broadening, and Zeeman broadening [34]. Natural line width is the frequency broadening due to the uncertainty in the energy of an excited quantum level. Doppler broadening is due to the frequency shift in the radiation emitted from a moving transmitter, or received by a moving receiver, which is transmitted to a receiver at a frequency f [34]. As the signal from a transmitter on a moving platform approaches a stationary receiver, this emitted radiation arrives at a higher frequency. Similarly, if the receiver is moving, there can be an increase or decrease in the received signal frequency. Zeeman broadening is the splitting of an atom or molecule's energy level when placed in a magnetic field [35]. The splitting of energy levels is known as the Zeeman effect and occurs in atmospheric pressures less than 10 mbar, corresponding to an altitude of 30 km or above.

Chapter 3 - Atmospheric Model

Recently, new observations in the vicinity of 60 GHz have been made. Out of this research came new equations and an empirical model with the capability to simulate the effects of dry air, water vapor, suspended droplets, and rain on a 50-70 GHz link. For the purposes of this thesis, only the effects of dry air are considered. Along with this model, the characteristics of a propagating radio wave are reviewed and the relationship between refraction, absorption, dispersion, refractive index, and field strength are presented.

3.1 Characteristics of a Propagating Radio Wave

Refraction, absorption, and dispersion affect the inherent characteristics of a radio wave propagating through the atmosphere. The field strength *E(z)* [36] is given by

$$E(z) = E(0)\exp\left[jkz\left(1 + N(f)\times 10^{-6}\right)\right] \quad (13)$$

which describes a plane radio wave traveling a distance *z*. *E(0)* is the initial amplitude of the wave, and

$$k = \frac{2\pi f}{c} \quad (14)$$

is the free space wave number, with *c* representing the speed of light in a vacuum. The complex refractivity *N(f)* is characterized by

$$N(f) = (n-1)\times 10^{6} = N_o + N'(f) + jN''(f) \quad (15)$$

where *N(f)* is in parts per million and the complex refractive index *n* is

$$n = n' - jn''. \quad (16)$$

The complex refractive index *n* is the ratio of the electromagnetic radiation in a vacuum to radiation in an atmospheric medium and depends on frequency and atmospheric conditions. The real part of *n* represents the reduction in propagation velocity whereas the imaginary part characterizes the loss of wave energy.

The refractive index exceeds unity by a small amount, on the order of 10^{-3}, thus it is more convenient to use the complex refractivity *N(f)*. At sea level, the complex refractivity *N(f)* is about 310 ppm. The parameter N_o represents the real nondispersive part and does not depend on frequency. The parameters *N□(f)* and *N□(f)* quantify the imaginary and real part of the dispersive complex refractivity, respectively. The imaginary part, *N□(f)*, contributes to power attenuation and the real part, *N□(f)*, contributes to phase dispersion and group delay, which is discussed in Section 3.2 [1], [2], [40].

3.2 Microwave Propagation Model (MPM)

After an extensive study, Hans J. Liebe published a model, the Microwave Propagation Model (MPM) in several journals beginning in the 1980s [36], [34], [37]. The MPM characterizes the behavior of attenuation and dispersion due to atmospheric oxygen and water. The attenuation and dispersion due to atmospheric oxygen in the frequency range of 50-70 GHz are considered here. In his model, Liebe presented the relationship between attenuation, dispersion, and complex refractivity. Most of the equations in this model are based on empirical results taken at the National Telecommunications and Information Administration [1]. Liebe's model is based on the work by Van Vleck and Rosenkranz [30], [32], [38].

The MPM model begins with the relationship between the complex refractivity, *N''(f)* and *N'(f)*, and power attenuation α, phase dispersion β, and group delay τ, which are expressed as

$$a(f) = 10^6 \left(\frac{4\pi}{c}\right) 10\log(e)\, f\, N''(f) = 0.1820\, f\, N''(f) \qquad (17)$$

$$\beta(f) = \left(\frac{2\pi}{c}\right) f\, N'(f) = 0.0210\, f\, N'(f) \qquad (18)$$

and

$$\tau = 3.3356\, N'(f) \qquad (19)$$

with the units of *f* in GHz, $\alpha(f)$ in dB/km, $\beta(f)$ in rad/km, and τ in ps/km. An electromagnetic wave traveling through an atmospheric medium suffers from group delay. Group delay causes the signal to arrive later than it would have if transmitted in a vacuum.

The presence of atmospheric oxygen in the link is represented by the transfer function

$$H_{O_2}(f) = A(f)\exp[jk\Phi(f)] \quad (20)$$

where $A(f)$ is the attenuation, k is the free space wave number (see equation (14)), and $\Phi(f)$ is the phase. The attenuation and phase components are expressed as

$$A(f) = \alpha(f) * L \quad (21)$$

and

$$\Phi(f) = \beta(f) * L \quad (22)$$

where L is the distance of the link, $\alpha(f)$ is from equation (17) and $\beta(f)$ is from equation (18).

3.2.1 Nondispersive Refractivity

In the MPM, N_o represents the nondispersive refractivity, which is discussed in Section 2.2.2 and is the sum of four parameters that correspond to different atmospheric behavior. N_o is expressed as

$$N_o = N_1 + N_2 + N_3 + N_4 \quad (23)$$

where

$$N_1 = 2.588\, p\theta \quad (24)$$

$$N_2 = (41.63\theta + 2.39)e\theta \quad (25)$$

$$N_3 = W\left(\frac{3}{2}\right)\left(1 - \frac{3}{\varepsilon_0 + 2}\right) \quad (26)$$

and

$$N_4 \approx R\frac{(3.7 - 0.012R)}{k_R}. \quad (27)$$

The temperature T is converted into a relative inverse temperature variable θ that is represented by

$$\theta = \frac{300}{T} \quad (28)$$

where T is in Kelvins. Barometric pressure P (mbar) is the sum of the partial pressures for dry air p (mbar), and water vapor e (mbar). The partial pressure for water vapor e is expressed as

$$e = \frac{v}{7.223\theta} \quad (29)$$

where (g/m^3) is the water vapor concentration and is the relative inverse temperature variable. The dry air partial pressure p is expressed as

$$p = P - e \quad (30)$$

where e is the water vapor partial pressure and P is the atmospheric pressure. N_1, N_2, N_3, and N_4 represent the nondispersive refractivity of dry air, water vapor, suspended droplets, and rain, respectively. The terms N_1 and N_2 are often known as the "dry" and "wet" terms of clear air propagation through the atmosphere. The simulation discussed in the following chapter considers only the effect of dry air and uses the following equation:

$$N_o = N_1 . \quad (31)$$

3.2.2 Attenuation and Dispersion

The complex refractivity, *N(f)*, includes the effects of local line resonance contributions, dry air nonresonant spectra, water vapor continuum spectra, suspended water-droplet refractivity, and rain approximation. For this project, only the dry air conditions are simulated, so only the local line resonance contributions (N_L) and dry air nonresonant spectra (N_D) are considered [1]. The local line resonance contributions determine the shape of the attenuation, phase, and group delay plots, whereas the nonresonant atmospheric oxygen spectrum is due to the dry air nonresonant spectra at ground level pressure.

The local line resonance contributions (N_L) and dry air nonresonant spectra (N_D) are complex quantities and are related to the complex refractivity, *N'(f)* and *N''(f)*, as follows:

$$N''(f) = N''_L(f) + N''_D(f) \quad (32)$$

and

$$N'(f) = N'_L(f) + N'_D(f) \quad (33)$$

where local line contributions, $N'_L(f)$ and $N''_L(f)$, and dry air nonresonant spectra, $N'_D(f)$ and $N''_D(f)$, are discussed in Sections 3.2.2.1 and 3.2.2.2, respectively.

3.2.2.1 The Local Line Contributions

Local line resonance is due to coupling between adjacent rotational states in molecular collisions. When the pressure increases, more molecular collisions occur causing individual line contributions to overlap and create a smooth-shaped spectrum centered on 60 GHz (see Figures 3.1 through 3.5). The line shape function in Liebe's model is based on Van-Vleck's shape function equation (3), which was later modified to include the effects of line overlap [38], [39]. The individual local resonance lines are seen in the attenuation and phase dispersion curves in Figure 3.1 and Figure 3.2, respectively. As the pressure increases, the individual lines couple with neighboring resonance lines, as seen in Figure 3.3 and Figure 3.4, until the individual lines are no longer present, as seen in Figure 3.5 and Figure 3.6.

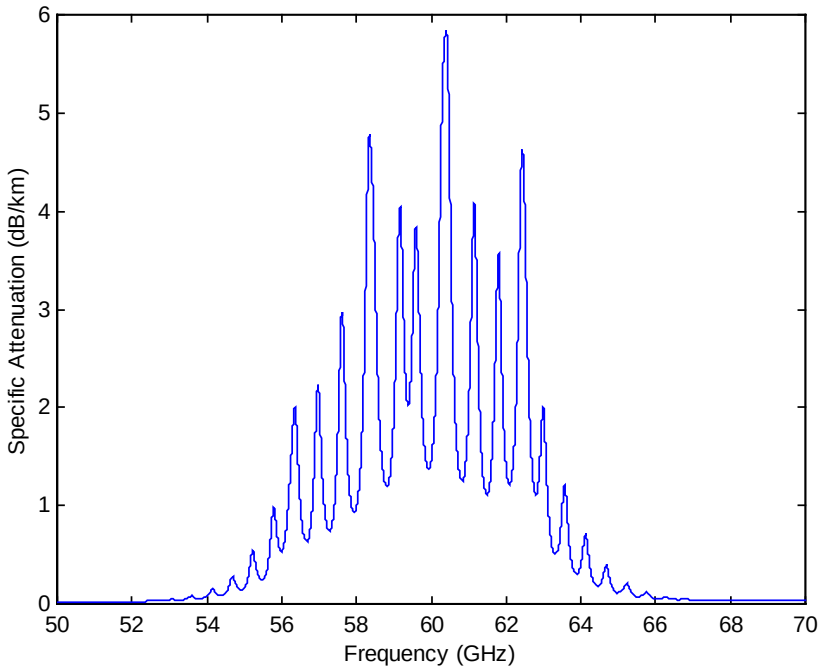

Figure 3.1 - Specific attenuation of atmospheric oxygen at a pressure of 75 mbar and an altitude of 18 km (59,400 ft) based on a standard atmosphere.

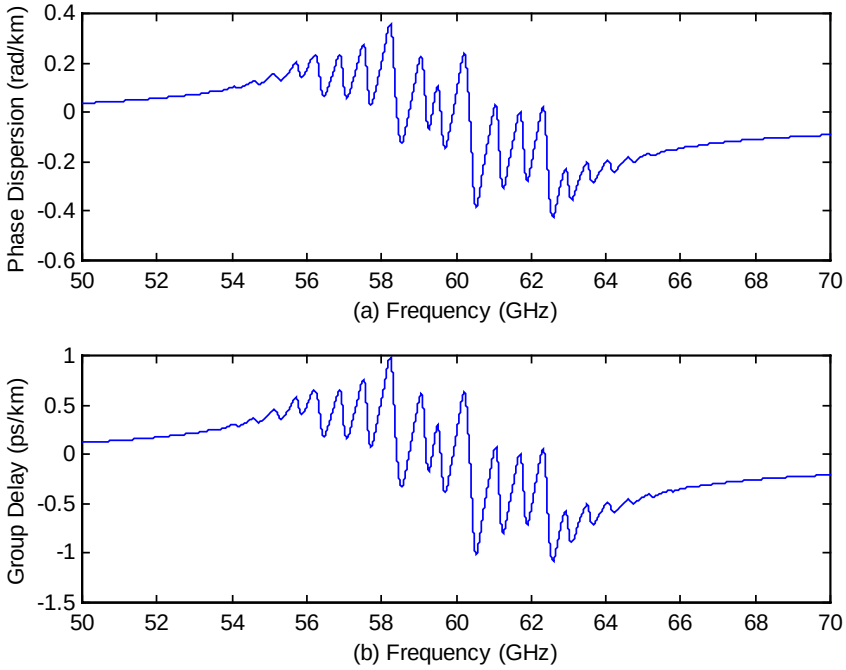

Figure 3.2 - Phase dispersion (a) and group delay (b) of atmospheric oxygen at $P = 75$ mbar.

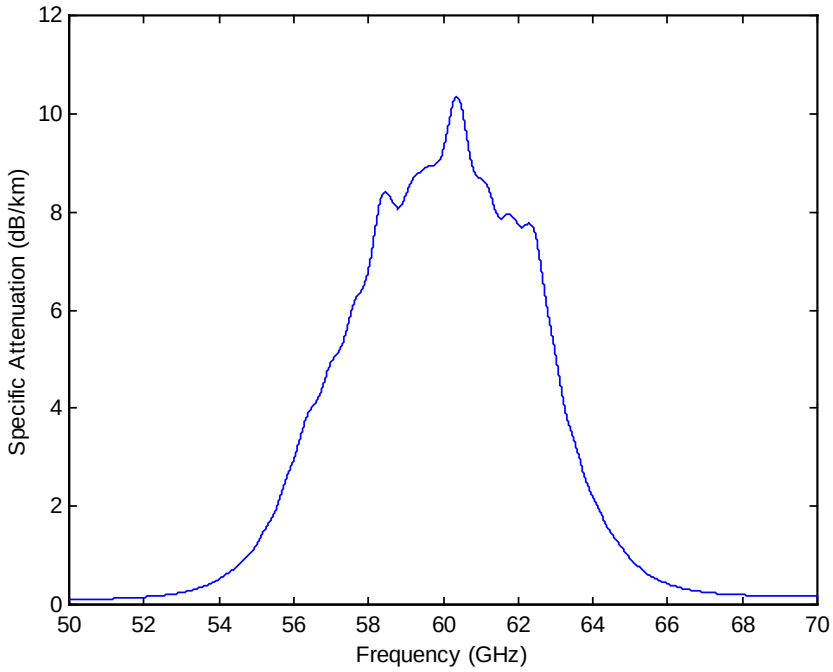

Figure 3.3 - Specific attenuation of atmospheric oxygen at a pressure of 310 mbar and an altitude of 9 km (29,700 ft) based on a standard atmosphere.

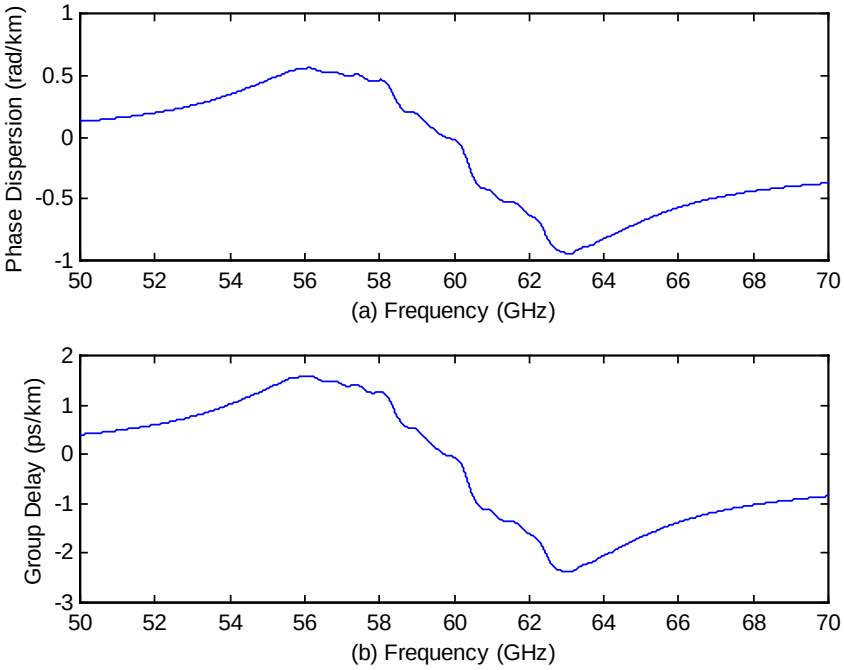

Figure 3.4 - Phase Dispersion (a) and Group Delay (b) of Atmospheric Oxygen at P = 310 mbar

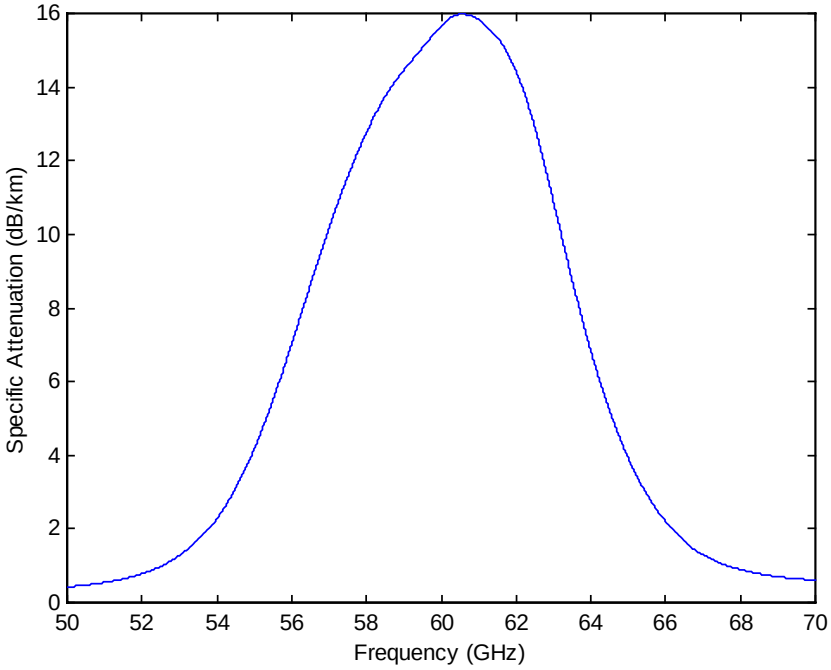

Figure 3.5 - Specific attenuation of atmospheric oxygen at a pressure of 1013 mbar found at sea level and is based on a standard atmosphere.

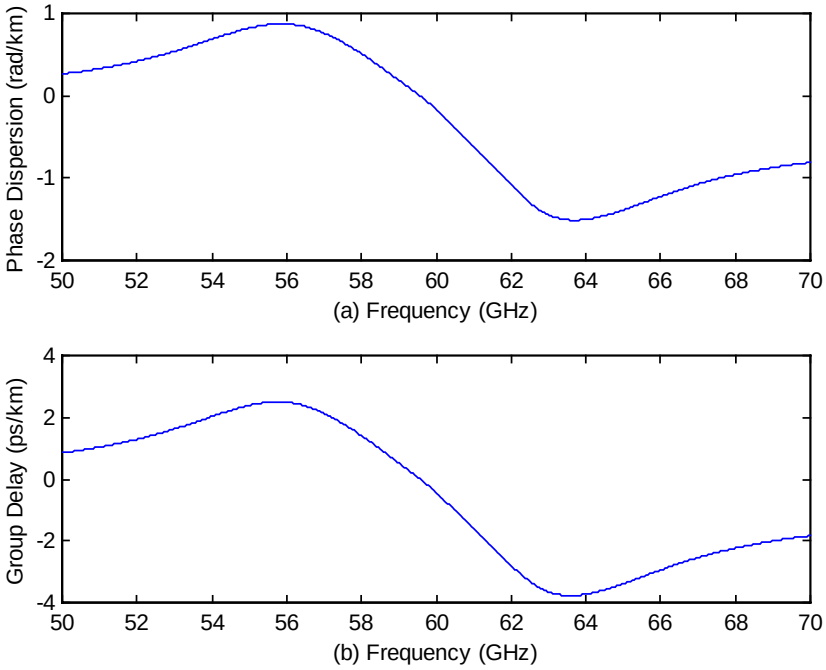

Figure 3.6 - Phase dispersion (a) and group delay (b) of atmospheric oxygen at *P* = 1013 mbar.

Liebe presents the shape function in a simplified form as compared to the equations presented in earlier publications by various authors [1]. The local line resonance contributions are calculated as a line-by-line summation $N_L(f)$ of the product of the complex shape function $F(f)$ and the line strength S for each of the 37 O_2 lines in the vicinity of 60 GHz. The line-by-line calculation is

$$N_L = \sum_{i=1}^{37} S_i F_i(f) \qquad (34)$$

with

$$F(f) = F'(f) - iF''(f) \qquad (35)$$

where i is the index, $F(f)$ is in GHz^{-1}, and S is in kHz. The line spectra for absorption (F'') and for dispersion (F') are given by

$$F''(f) = \left(\frac{\gamma f}{f_o}\right)\left(\frac{1}{(f_o - f)^2 + \gamma^2} + \frac{1}{(f_o + f)^2 + \gamma^2}\right) - \left(\frac{\delta f}{f_o}\right)\left(\frac{f_o - f}{(f_o - f)^2 + \gamma^2} + \frac{f_o + f}{(f_o + f)^2 + \gamma^2}\right) \qquad (36)$$

and

$$F'(f)=\frac{\left(\left(f_o^{\,2}+\gamma^2\right)/f_o\right)-f}{(f_o-f)^2+\gamma^2}+\frac{\left(\left(f_o^{\,2}+\gamma^2\right)/f_o\right)+f}{(f_o+f)^2+\gamma^2}-\frac{2}{f_o}+\delta\left(\frac{f\gamma}{f_o}\right)\left(\frac{1}{(f_o-f)^2+\gamma^2}-\frac{1}{(f_o+f)^2+\gamma^2}\right) \quad (37)$$

where f_o is in GHz and is the center frequency for each of the resonance lines. The strength of each individual resonance line is characterized by

$$S=a_1 10^{-6}\, p\theta^3 e^{[a_2(1-\theta)]} \quad (38)$$

where a_1 is in kHz/mbar, a_2 is unitless, and e is the water vapor partial pressure. The remaining line parameters are the pressure-broadened width $\square$[2] in GHz

$$\gamma=a_3 10^{-3}\left(p\theta^{(0.8-a_4)}+1.1e\theta\right) \quad (39)$$

and the pressure induced interference $\square$

$$\delta=(a_5+a_6\theta)10^{-3}\, p\theta^{0.8} \quad (40)$$

where $\square$ and a_4 are unitless, a_3 is in GHz/mbar, and a_5 and a_6 are in mbar^{-1}. The pressure-broadened width is the bandwidth of each individual resonance line. As pressure increases, the widths of individual resonance lines broaden or spread to neighboring lines. As these lines spread, the appearance of individual lines disappears. The pressure-induced interference variable accounts for this broadening behavior in the line shape functions (36)and (37). Liebe obtained the parameters $a_{1\text{-}6}$ and f_o from laboratory measurements, which are presented in Table A.1 in Appendix A.

3.2.2.2 Dry Air Nonresonant Spectrum

Dry air nonresonant refractivity $N_D(f)$ contributes a small amount to the complex refractivity at ground level pressure due to the nonresonant O_2 spectrum below 10 GHz and the pressure-induced nitrogen absorption above 100 GHz. The Debye spectrum of atmospheric oxygen is considered the relaxation of the spectrum due to atmospheric oxygen's magnetic dipole moment [33]. The real and imaginary terms of $N_D(f)$, respectively, are

$$N_D'(f)=S_d\left(\frac{1}{1+(f/\gamma_o)^2}-1\right) \quad (41)$$

[2] In Chapter 2, $\square$ represents oxygen absorption in dB/km but in this chapter, $\square$ represents the pressure-broadened width in GHz.

and

$$N_D''(f) = \frac{S_d f}{\gamma_o}\left(1 + \left(\frac{f}{\gamma o}\right)^2\right) + a_p f p^2 \theta^{3.5} \qquad (42)$$

where

$$S_d = 6.14 * 10^{-4}\, p\theta^2 \qquad (43)$$

is the strength of the nonresonant contribution,

$$\gamma_o = 5.6 * 10^{-3}(p + 1.1e)\theta \qquad (44)$$

is the relaxation frequency, and

$$a_p = 1.40 * 10^{-10}\left(1 - 1.2 * 10^{-5} f^{1.5}\right) \qquad (45)$$

is the contribution from the N_2 absorption.

The local line resonance and dry air non-resonance components of the Microwave Propagating Model are used in the simulation process discussed in Chapter 4. For further explanations and equations of the suspended water-droplet refractivity and the rain approximation see references [1], [40].

Chapter 4 - Simulation

Computer programs were written to simulate and visualize the effects of attenuation and dispersion due to the atmospheric oxygen on a wideband digital link. (See Appendix A for MATLAB code.) Before understanding the simulation process, the background for the code needs to be presented. In this chapter, the communication system, including the block diagram, is discussed so that the reader can understand the flow of the simulation code. In previous chapters, inter-symbol interference (ISI) was mentioned, but its significance in a communication link was not discussed until now. The effect of the atmosphere on a digital signal is presented, as well as the transfer functions that describe this atmospheric effect. The chapter concludes with a discussion of the simulation process.

4.1 Communication System

The communication system used in this simulation, which is presented in Section 4.4, includes three components: the transmitter, the link, and the receiver. The block diagram for the communication system is shown in Figure 4.1.

The transmitter includes three blocks: the bit generator, the +/- 1V block, and the BPSK modulator. The bit generator generates a digital signal with each bit having a voltage level of either 0 V or 1 V. The +/- 1V block converts the voltages of 0V and 1V to –1V and 1V, respectively. The BPSK modulator consists of a mixer and an oscillator with oscillating frequency f_c.

The block diagram in Figure 4.1 does not include power amplifiers, frequency converters, etc., which are normally considered in the design of physical radios. In the frequency domain, power amplifiers and frequency converters perform linear operations. It is assumed that there is a linear relationship between the transmitter and the link sections, so the blocks for power amplifiers and frequency converters are not included.

Two Nyquist square root raised cosine (RRC) filter blocks and an atmosphere, or link, block represent the link portion. The Nyquist filters are based on theory and are placed in the link to eliminate ISI introduced by the communication system. The link block represents the effects of the atmosphere on the signal.

The receiver components begin with the BPSK demodulator and continue with a band-pass filter and a comparator with a threshold voltage of 0V. Finally, the output is displayed to check against the original signal sent. An eye diagram is included to examine each bit before it passes through the comparator.

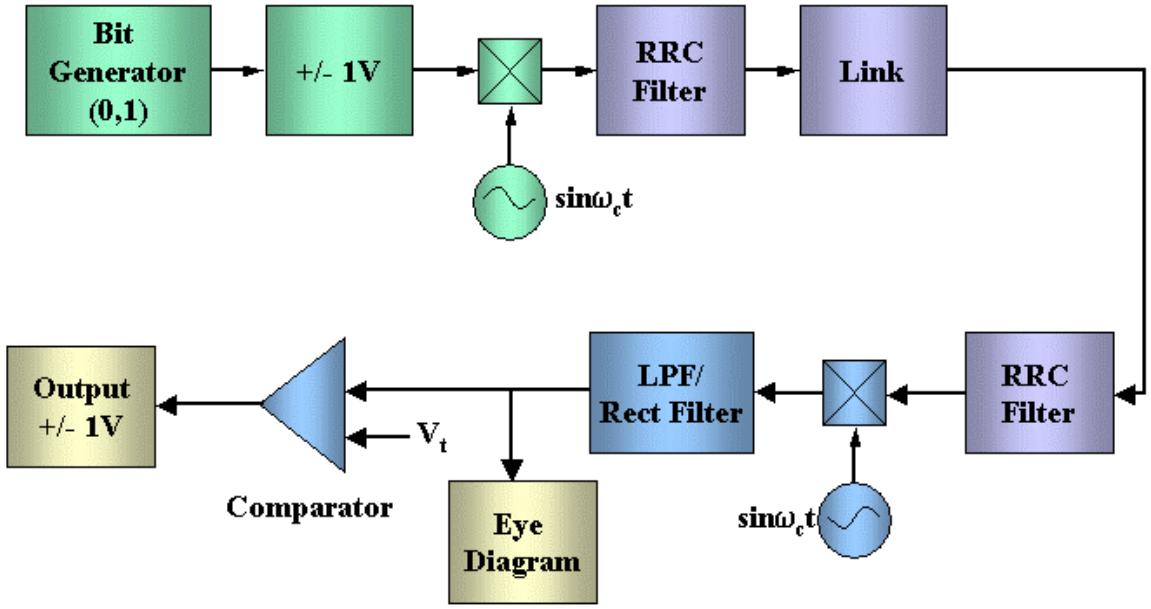

Figure 4.1 - Block Diagram

4.2 ISI in Digital Links

Atmospheric gases, especially atmospheric oxygen in the 50-70 GHz band, affect the signal both in magnitude and in phase. If the phase of the signal is affected, the possibility of ISI in the received signal is very likely. ISI occurs if the pulses are not filtered correctly as the signal passes through the communication system. As a result of the pulses not being filtered properly, these pulses spread into neighboring time slots over time [41] as if the pulses are distorted as they pass through the link. Since there is a chance that ISI can occur in the system, a zero ISI communication link needs to be designed.

To approach the requirements of a zero ISI link, the transfer function (TF) of the link must approximate a filter shape similar to the RRC filter and the transmitter must send short pulses instead of impulses [42]. In this simulation, the short pulses are represented by NRZ waveforms that have nulls spaced $1/T_s$ Hz apart, where T_s is the symbol period. The RRC-like filters are bandpass filters centered on f_c with an occupied bandwidth, B, of

$$B = B_{occ} = R_s(1+\alpha) \quad (46)$$

where R_s is the symbol rate and α is the roll-off factor.

To correct the shape of the input spectrum, an equalizer filter is included after the BPSK modulator. For NRZ pulses, the transfer function of the equalizer needs to be the inverse of the input spectrum so that the output spectrum will be flat over the occupied bandwidth of the link. The requirement for zero ISI is that the system (input to output) transfer function be a Nyquist transfer function. The system transfer function is expressed as

$$V_r(f) = V_t(f) \times \sqrt{H_e(f)} \times E_q(f) \times H_L(f) \times \sqrt{H_e(f)} = H_e(f) \quad (47)$$

where $V_t(f)$ is the input spectrum, $H_e(f)$ is the RRC filter TF (one for the transmitter and one for the receiver), $E_q(f)$ is the equalizer TF, and $H_L(f)$ is the link TF. In order for (46) to be valid, $V_t(f) \times E_q(f) = 1$ and $H_L(f) = 1$ must hold.

4.3 Effects of the Atmosphere

Atmospheric oxygen causes attenuation and phase dispersion in digital signals propagating through the atmosphere if the transmitting frequency is in the vicinity of 60 GHz. For communication systems with small bandwidths, the phase dispersion due to atmospheric oxygen has little or no impact on the phase of digital signals. For wideband signals, phase dispersion changes the phase slightly but enough to introduce ISI and/or bit errors into the digital signal.

Attenuation due to atmospheric oxygen reduces the strength of the signal by a maximum of 16 dB/km, depending on pressure and temperature conditions. If a signal is not received, then the attenuation may be more than is allowed for in the link budget. If a digital signal is weakened by attenuation, bit errors still occur if the receiver detects bits incorrectly.

Atmospheric pressure also affects digital signals. At higher pressures, atmospheric oxygen causes considerable attenuation and a small time delay in the received digital signal, as seen in the eye diagram of Figure 4.2. But at lower atmospheric pressures, atmospheric oxygen

causes phase distortion in the signal, which results from the presence of individual resonances lines, as seen in the eye diagram of Figure 4.3. The center of the eye diagram is farther away from the center of the symbol period in Figure 4.3 than in Figure 4.2. The information presented in Figure 4.2and Figure 4.3 is discussed in more detail in Chapter 5.

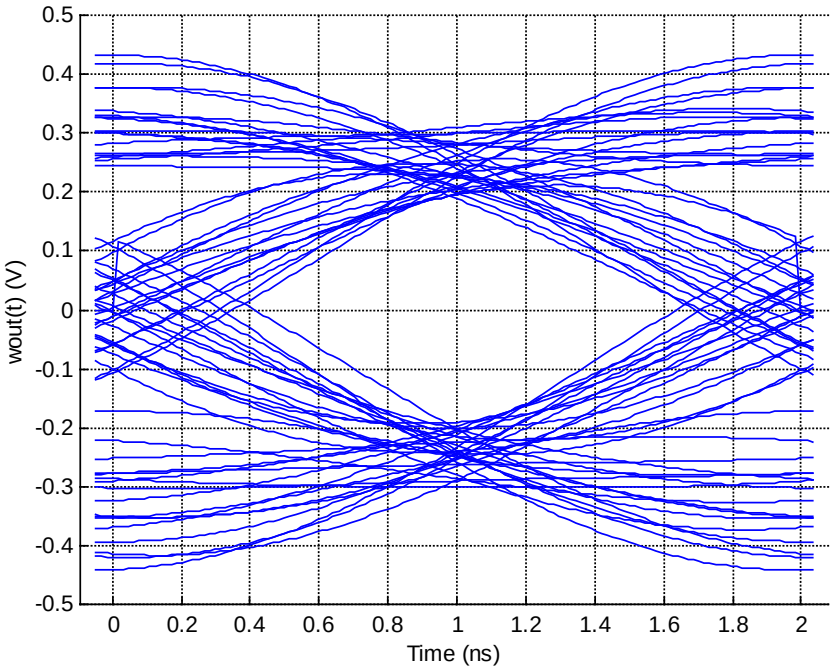

Figure 4.2 - Eye Diagram with Atmospheric Oxygen Present in the Link with P = 1013 mbar, R_b = 0.5 Gbps, and d = 1 km.

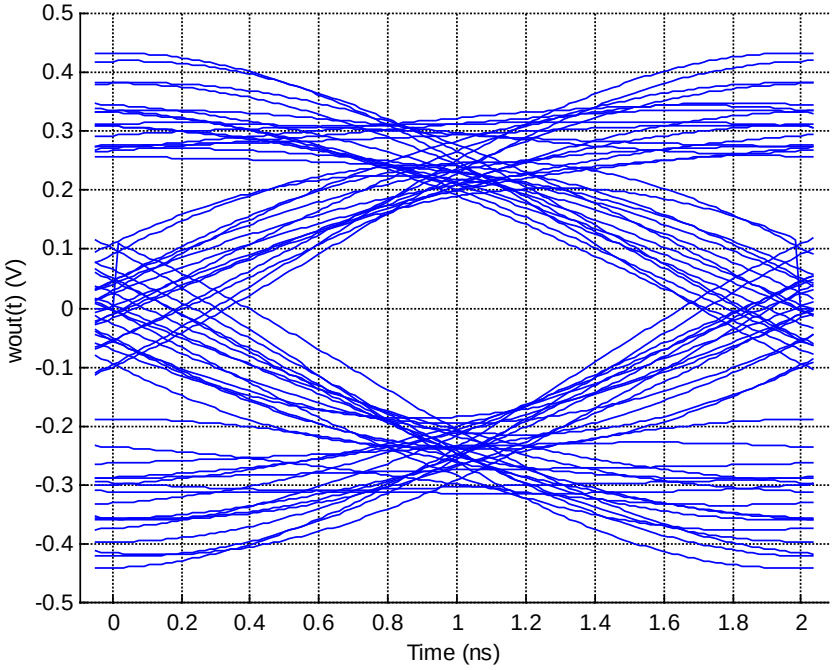

Figure 4.3 - Eye Diagram with Atmospheric Oxygen Present in the Link with P = 75 mbar, R_b = 0.5 Gbps, and d = 1 km.

4.4 Simulation Process

This section describes the simulation process used in determining the effect of atmospheric oxygen on a wideband digital signal. The reader may find it useful to refer to the block diagram on page 34.

4.4.1 Initial System Parameters

Table 4.1 lists the system parameters used in this simulation. The parameter 2^m refers to the number of symbols generated by the bit generator, where m has unitless values between 3 and 6. The symbol period T_s has values between 0.5 ns and 2 ns depending on the bit rate, since $R_b = 1 / T_s$. This simulation tests data rates ranging from 0.5 Gbps to 2 Gbps. The occupied bandwidth ranges between 0.625 GHz and 2.50 GHz for a RRC filter roll-off factor of □ = 0.25. The carrier frequency is 60 GHz.

Table 4.1 - Initial System Parameters

Parameter	*Variable*	*Values*	*Units*
Power of 2	m	3 to 6	(Unitless)
Number of Symbols	2^m	8 to 64	(Unitless)
Symbol Period	T_s	0.5 to 2	ns
Bit Rate	R_b	0.5 to 2	Gbps
Roll-off Factor	α	0.25	(Unitless)
Occupied Bandwidth	$B = R_b * (1 + \alpha)$	0.625 to 2.50	GHz
Carrier Frequency	f_c	60	GHz

4.4.2 Digital Signal

NRZ waveforms were used to represent the short pulses needed to achieve a zero ISI in the link. A 2^m random unipolar non-return to zero (NRZ) waveform ($x(t)$) was generated in the time domain using the random number generator in MATLAB, where

$$x(t)=\begin{Bmatrix} 0V, & if\ symbol\ is\ 0 \\ 1V, & if\ symbol\ is\ 1 \end{Bmatrix}. \quad (48)$$

Once the waveform was generated it was then converted to a polar NRZ waveform ($m(t)$) where a voltage level of 0 became –1 V and a voltage level of 1 became +1 V.

$$m(t)=\begin{Bmatrix} -1V, & if\ symbol\ is\ 0 \\ +1V, & if\ symbol\ is\ 1 \end{Bmatrix} \quad (49)$$

4.4.3 BPSK Modulator

After generating a random sequence of bits, the signal is modulated using Binary Phase-Shift Keying (BPSK). A BPSK signal with phase shift of ±□/2 is characterized[3] as [41]

$$s(t)=-A_c m(t)\sin\omega_c t \quad (50)$$

where A_c is the magnitude of the waveform, □$_c$ is the oscillator frequency, and $m(t)$ is a polar baseband data signal. Equation (50) is the optimum case and is used for the simulation of this project.

[3] See Section 5-9 in Couch's text [41] for a description of a BPSK signal.

For this simulation, conventional BPSK is used with an amplitude $A_c = 1$; the polar data stream $m(t)$ from the previous section; and the carrier frequency $\omega_c = 2\pi f_c$. Once the BPSK signal is generated, the signal is converted to the frequency domain using the Fourier Transform, which makes the computation more manageable when dealing with the filters and the atmospheric model.

4.4.4 System Transfer Functions

The Nyquist transfer functions used to achieve a zero ISI link are slightly modified for this simulation. The RRC filters are centered on f_c and the filter transfer function becomes

$$H_e(f) = \begin{cases} 0, & f \le f_c - B \\ \frac{1}{2}\left\{1 + \cos\left[\frac{\pi(f - (f_c + f_1))}{2f_\Delta}\right]\right\}, & f_c + f_1 < f < f_c + B \\ 1, & f_c - f_1 \le f \le f_c + f_1 \\ \frac{1}{2}\left\{1 + \cos\left[\frac{\pi(f - (f_c - f_1))}{2f_\Delta}\right]\right\}, & f_c - B < f < f_c - f_1 \\ 0 & f \ge f_c + B \end{cases} \quad (51)$$

The parameters f_1 and f_Δ are defined as

$$f_\Delta = B - f_o \quad (52)$$

and

$$f_1 = f_o - f_\Delta \quad (53)$$

with f_o being the 6-dB bandwidth of the filter. The bandwidth B is defined in equation (46). The equalizer function is also centered on f_c and is represented by

$$Eq(f) = \frac{\pi T_s (f - f_c)}{\sin(\pi T_s (f - f_c))} \quad (54)$$

where the bandwidth of the TF is f_c-$0.5R_s$ to f_c+$0.5R_s$.

For the purposes of this project, a zero ISI link without multipath or fading is assumed for this radio link. Thus the link is also assumed to be linear and to have a link transfer function of $H_L(f) = 1$. Since the link is assumed to be linear and have zero ISI, the only distortion introduced at the receiver comes from the effects of atmospheric oxygen in the link. The transfer function at the receiver becomes the transfer function of the Nyquist filter $H_e(f)$ times the atmospheric oxygen transfer function $H_O(f)$. Equation (47) becomes

$$V_r(f) = V_t(f) \times \sqrt{H_e(f)} \times E_q(f) \times H_L(f) \times H_O(f) \times \sqrt{H_e(f)} = H_e(f) \times H_O(f). \quad (55)$$

4.4.5 Atmospheric Oxygen Attenuation and Dispersion

Using the information presented in Chapter 3, the transfer function of the atmospheric portion of the RF communication link is

$$H_{O_2}(f) = A(f)\,exp[jk\Phi(f)] \quad (56)$$

where $A(f)$ is the attenuation in equation (21), k is the free space wave number in equation (14) and $\Phi(f)$ is the phase in equation (22). The pressure and temperature are varied to examine the atmospheric oxygen spectrum at different altitudes using a standard atmosphere. The parameters are listed in Table 4.2 with the altitude ranging from 0 to 18 km, the atmospheric pressure from 75 to 1013 mbar and the temperature from -56 to 15 ºC.

Table 4.2 - Atmospheric oxygen Model Parameters

Parameter	*Symbol*	*Range*
Altitude	H	0 to 18 km
Barometric Pressure	P	75 to 1013 mbar
Temperature	T	-56 to 15 ºC

4.4.6 BPSK Demodulator and Low Pass Filter

Now the signal is demodulated in order to receive the information sent. The received waveform is multiplied by $sin\,\omega_c t$ to demodulate the signal and filtered through a bandpass filter to see if it was the original information sent. The demodulated signal $r(t)$ becomes

$$r(t) = -A_c\, v_r(t)\, sin(\omega_c t) \quad (57)$$

where $v_r(t)$ is the received waveform. The demodulated spectrum $R(f)$ is filtered to eliminate the high frequency components. For the bandpass filter, a Nyquist RRC filter is used and is expressed by

$$H_e(f) = \begin{cases} 1, & |f| < f_1 \\ \frac{1}{2}\left\{1 + cos\left[\frac{\pi(|f| - f_1)}{2f_\Delta}\right]\right\}, & f_1 < |f| < B \\ 0, & |f| > B \end{cases} \quad (58)$$

The center frequency of the filter is f = 0 Hz and B is the occupied bandwidth. The output spectrum $W_{out}(f)$ is

$$W_{out}(f) = R(f) \times H_{BP}(f) \quad (59)$$

where $H_{BP}(f)$ is the bandpass filter.

4.4.7 Eye Diagram

An eye diagram is used to visualize how atmospheric oxygen attenuation affects the link. An eye diagram repeatedly plots the waveform of each symbol, plus a fraction of the waveform from neighboring symbols. If the eye is open, then bit errors did not occur in the waveform. If noise or ISI exists, the eye begins to close and bit errors are produced at the output of the receiver. Figure 4.4 shows the eye diagram when the simulation does not include the atmospheric effects, whereas Figure 4.5 is the eye diagram when the atmospheric effects are included. The center of the eye is in the middle of the symbol period at 1 ns and the eye is wide open in Figure 4.4 and Figure 4.5.

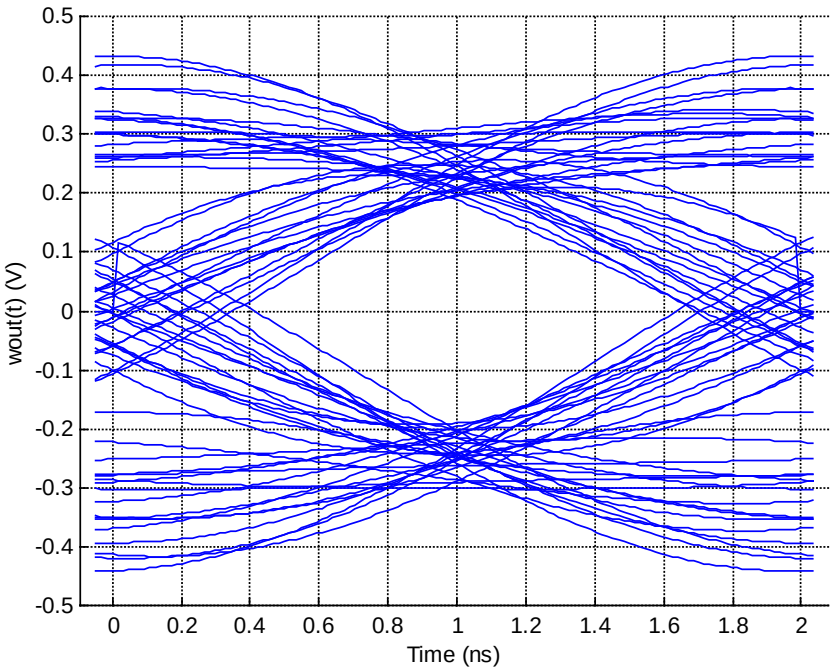

Figure 4.4 - Eye diagram without atmospheric oxygen present in the link.

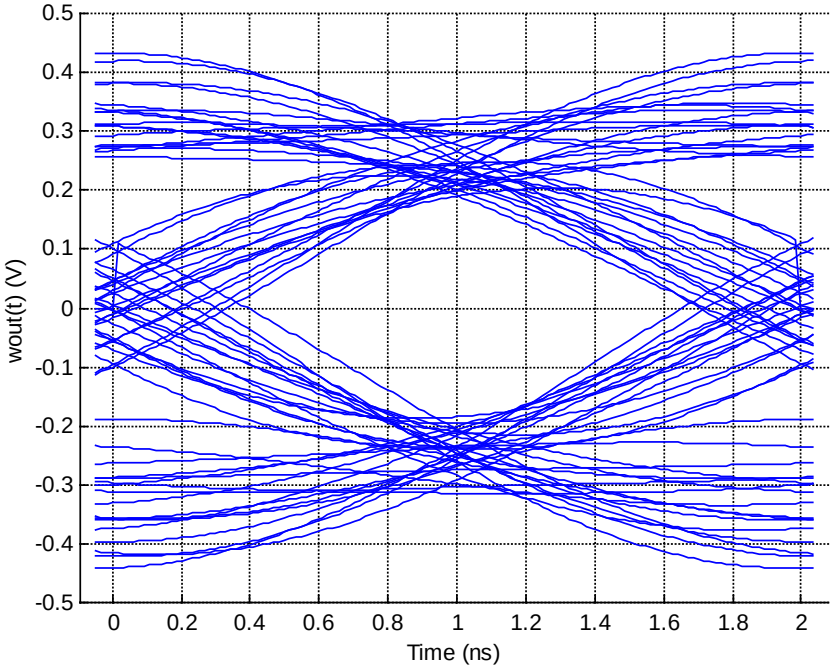

Figure 4.5- Eye Diagram with Atmospheric Oxygen Present in the Link with P = 75 mbar, R_b = 0.5 Gbps, and d = 1 km.

Chapter 5 - Results

So far, the theory [30] and the model [1] for characterizing the molecular resonance behavior of atmospheric oxygen, the atmospheric simulator, and several applications [5] for the use of the 60 GHz band have been introduced. The results in this chapter complement the information provided about the theory and the model and validate the simulation program. This chapter begins with a presentation of results based on a set of initial conditions and continues with explanations of how altering these conditions affect the results. The reader may find the block diagram (see Figure 4.1) helpful when attempting to visualize the simulation of the plots discussed in this chapter.

5.1 Results with Initial Conditions

The plots in this section are based on a set of initial conditions listed in Table 5.1. The data rate chosen is characteristic of a wideband or broadband system and is not necessarily associated with a particular standard. The pressure and temperature were selected as initial conditions since 1013 mbar and 15 °C (59 °F) are the standard atmospheric pressure and temperature at sea level, respectively [43]. The link is examined using a range of 1 km, which is a likely range for a signal operating in the 60 GHz band.

Table 5.1- Initial Conditions

Parameter	*Symbol*	*Value*
Data Rate	R_b	500 Mbps
Pressure	P	1013 mbar
Temperature	T	15 °C
Altitude	H	0 km
Range	d	1 km

5.1.2 Atmospheric Oxygen Attenuation

The first set of plots describes the specific attenuation, dispersion, and group delay of atmospheric oxygen using the initial parameters listed in Table 5.1. The plot for the specific attenuation of atmospheric oxygen is presented in Figure 5.1. The curve for the attenuation due to atmospheric oxygen is the result of evaluating equation (17), where the range of frequency, f, is from 50 to 70 GHz. The oxygen molecule resonates around 60 GHz resulting in a peak in the attenuation curve as seen in Figure 5.1. As the pressure decreases, the presence of individual resonance lines begin to appear in the attenuation curve, which is discussed in Section 5.2.

Atmospheric oxygen also contributes phase dispersion and group delay to a wideband signal, which is seen in Figure 5.2. In Figure 5.2, the phase change is smooth between 50 GHz and 70 GHz, but as atmospheric pressure decreases the phase changes occur more rapidly and individual peaks appear. Even at 310 mbar, the peaks of individual resonance lines appear in the attenuation plot of Figure 5.3. The effects of atmospheric oxygen attenuation at P = 310 mbar are discussed in Section 5.2.1.

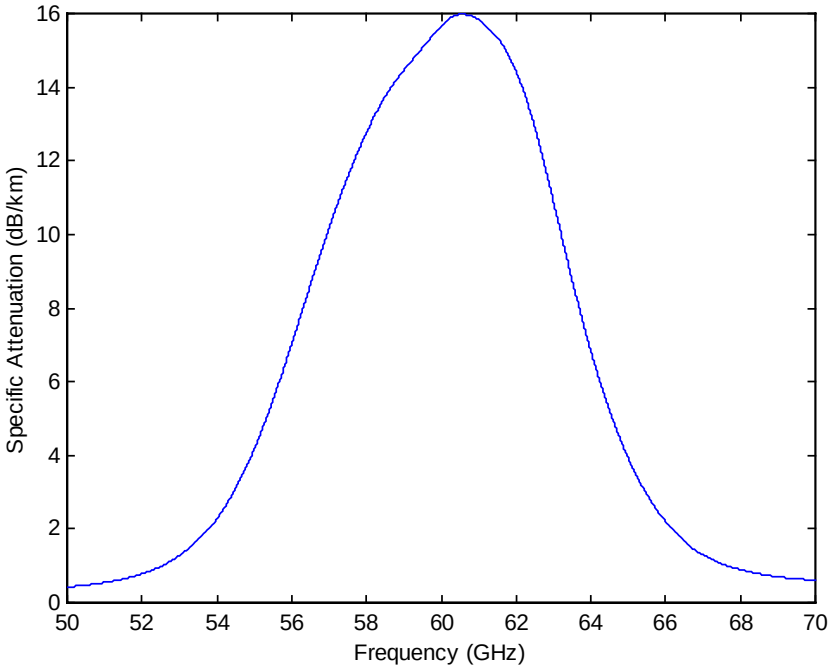

Figure 5.1 - Specific attenuation of atmospheric oxygen at a pressure of 1013 mbar found at sea level based on a standard atmosphere.

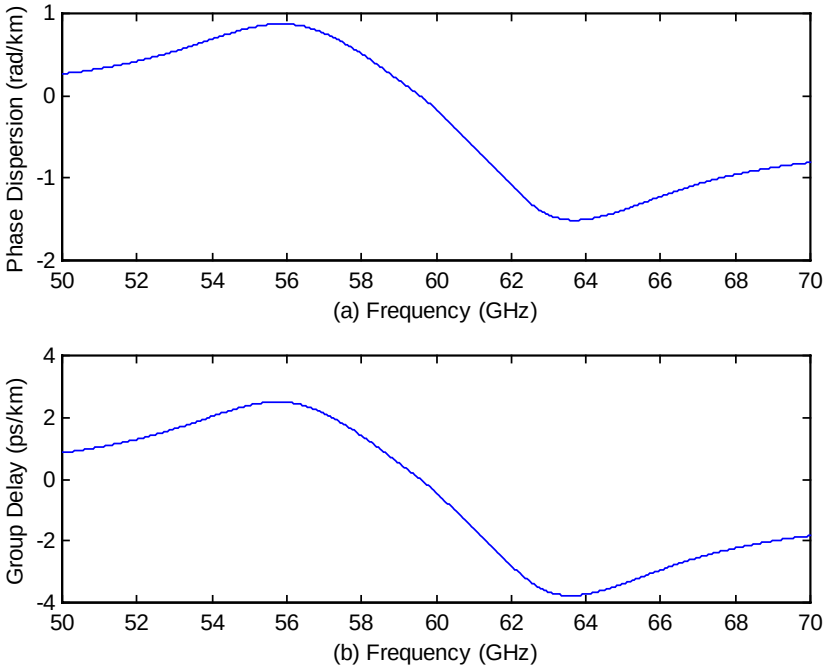

Figure 5.2 - Phase dispersion (a) and group delay (b) of atmospheric oxygen at P = 1013 mbar.

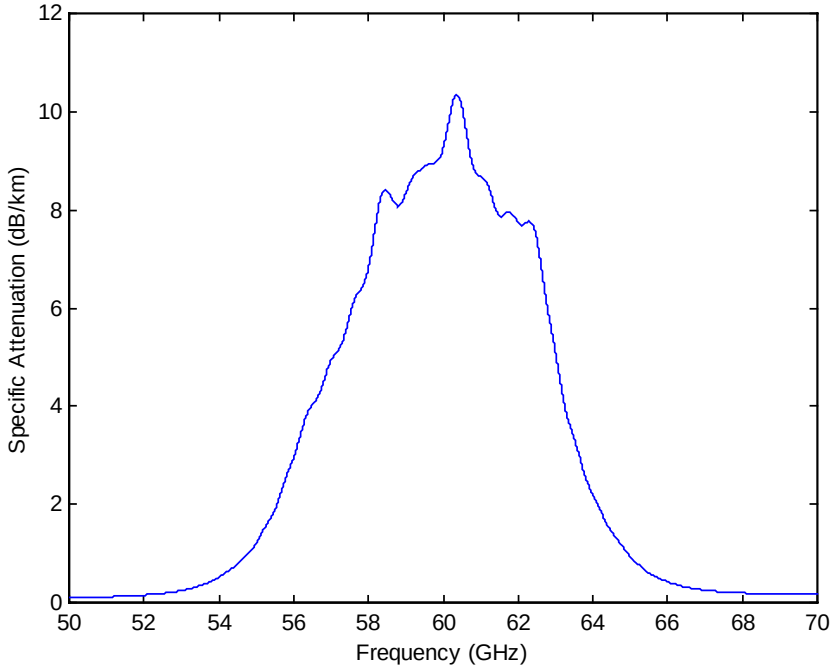

Figure 5.3 – Specific attenuation of atmospheric oxygen at a pressure of 310 mbar and an altitude of 9 km (29,700 ft) based on a standard atmosphere.

5.1.3 Eye Diagram

An eye diagram is used to visualize the effects of atmospheric oxygen on the signal and the presence of ISI in the waveforms. As seen in the block diagram (see Figure 4.1), the input to the eye diagram is the signal coming from the lowpass filter in the receiver. The eye diagram is the result of examining the waveform of each symbol plus a fraction of the waveform from the previous and next symbols. For R_b = 500 Mbps, the center of the eye is located at t = 1 ns, which is the sample point (see Figure 5.4).

All of the eye diagrams presented in this chapter are plotted with the signal ($w_{out}(t)$) vs. time and are normalized (see Figure 5.5) to a peak voltage of v_{pk} = 0.45 V, which is the peak voltage of the waveform in Figure 5.4. Also, all of the eye diagrams present the waveforms for signals with 64 symbols.

In order to examine the effects of atmospheric oxygen attenuation in the link, Figure 5.5 and Figure 5.4 show the results of the simulation with and without the atmospheric oxygen transfer function, respectively. In Figure 5.5, the atmospheric pressure is 1013 mbar, the

distance of the link is 1 km, and the data rate is R_b = 500 Mbps. The difference between Figure 5.4 and Figure 5.5 is barely noticeable. Examining both eye diagrams carefully, the reader can see a change in some of the waveforms due to the small phase dispersion caused by atmospheric oxygen. In both diagrams, the peak voltage in the center of the eye is V_{center} = ~ 0.20 V and the width of the eye is Δt = 1.2 ns. With a decrease in pressure, the peak voltage in the center becomes smaller, which represents the occurrence of possible bit errors.

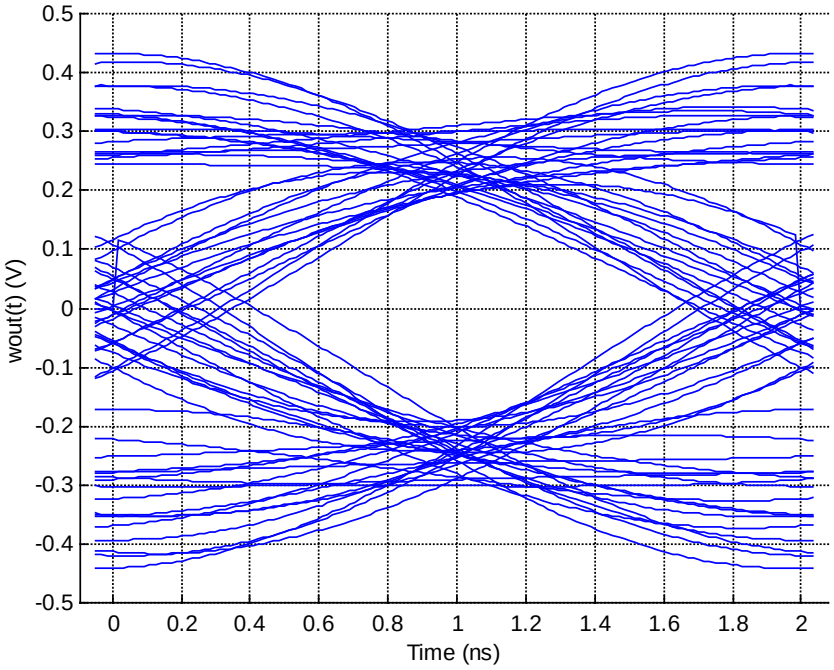

Figure 5.4 - Eye diagram without atmospheric oxygen present in the link.

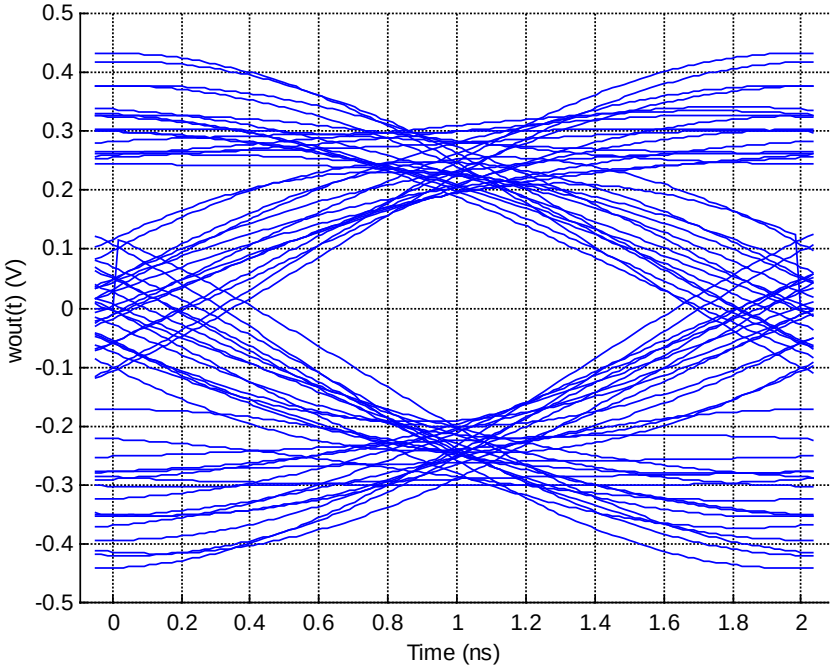

Figure 5.5 - Eye diagram with atmospheric oxygen present in the link with P = 1013 mbar, R_b = 0.5 Gbps, and d = 1 km.

5.2 Variable – Pressure

As discussed in Chapter 3, individual molecular resonance lines appear in the attenuation and phase dispersion curves as pressure decreases, which is seen in the figures presented in the following sections. In this section, the system is examined at two different atmospheric pressures, 310 mbar and 75 mbar. For both cases, the data rate (R_b = 500 Mbps) and the distance of the link (d = 1 km) remain constant over the frequency range of 50 GHz to 70 GHz.

5.2.1 Pressure at 310 mbar

At an atmospheric pressure of 310 mbar and an altitude of 9 km, the peaks of individual resonance lines are visible in the attenuation curve of Figure 5.6 and in the phase dispersion and group delay curves of Figure 5.7. The maximum attenuation due to atmospheric oxygen is about 11 dB/km at 310 mbar, which is significantly less than the 16 dB/km at 1013 mbar. As the pressure decreases, the individual lines become more prominent and do not contribute to neighboring lines, which results in less attenuation over the same frequency range.

The resonance behavior seen in the attenuation curve of Figure 5.6 is also replicated in Figure 5.7, where the ripples of individual lines appear. The peak phase dispersion and group delay have also decreased in magnitude in comparison to Figure 5.2. At higher pressures, individual lines contribute to neighboring lines and create the appearance of spreading, which results in more atmospheric oxygen attenuation, phase dispersion, and group delay. As the individual lines become distinguishable due to the decrease in pressure, the spreading effect is minimized and the lines contribute to the lower total attenuation individually.

Comparing Figure 5.4 with Figure 5.8, the difference is not noticeable. At this bandwidth, the impact of phase dispersion due to atmospheric oxygen on the signal is small. As the data rate increases, the impact of phase dispersion significantly affects the signal. The center peak voltage is about ~0.19 V and the width of the eye is Δt = 1.2 ns in both eye diagrams.

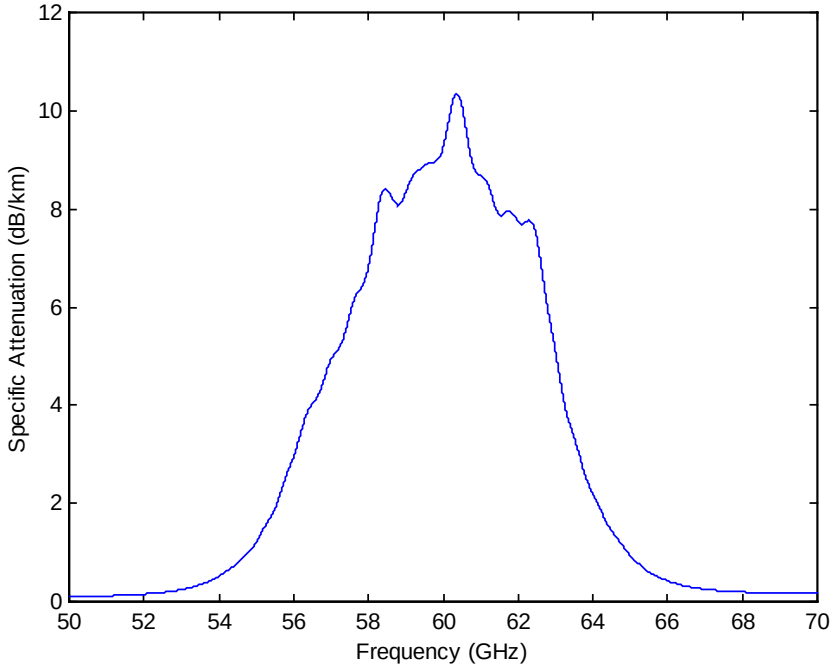

Figure 5.6 - Specific attenuation of atmospheric oxygen at a pressure of 310 mbar and an altitude of 9 km (29,700 ft) based on a standard atmosphere.

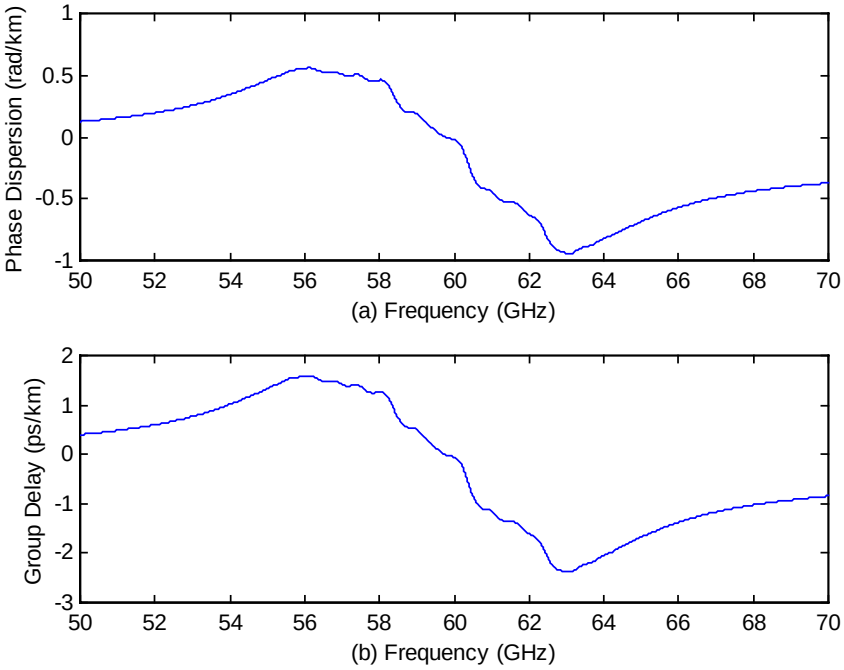

Figure 5.7 - Phase dispersion (a) and group delay (b) of atmospheric oxygen at $P = 310$ mbar

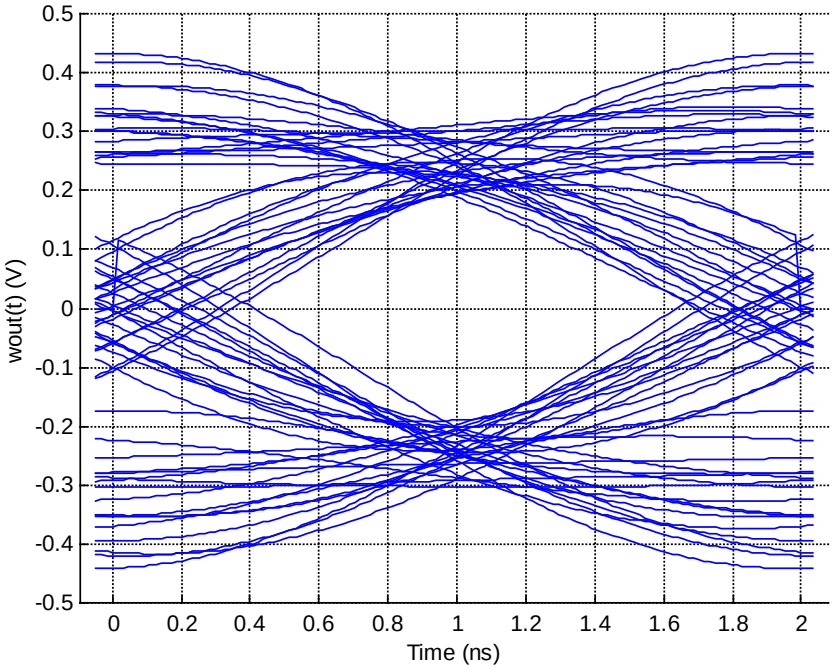

Figure 5.8 - Eye Diagram with Atmospheric Oxygen Present in the Link with $P = 310$ mbar, $R_b = 0.5$ Gbps, and $d = 1$ km.

5.2.2 Pressure at 75 mbar

At 75 mbar, which corresponds to an altitude of 18 km, the individual resonance lines are very pronounced, as seen in Figure 5.9 and Figure 5.10. The peak attenuation is less than 6 dB/km and the curve has over 20 individual resonance lines. When compared to Figure 5.1, the maximum attenuation is less for an atmospheric pressure of 75 mbar than for an atmospheric pressure of 1013 mbar over the frequency range of 50 GHz to 70 GHz. Individual resonance lines produce rigid waveforms in Figure 5.10, which represent rapid changes in phase and time, unlike the smooth plots of Figure 5.2.

In Figure 5.11, absorption at P = 75 mbar minimizes spreading in the eye diagram, which is seen when compared with Figure 5.4. The center peak voltage is still V_{center} = ~0.19 V and the width of the eye Δt = 1.2 ns remains constant. As the data rate increases, the impact of spreading in the signal is minimized, revealing a relatively clean eye diagram for P = 75 mbar.

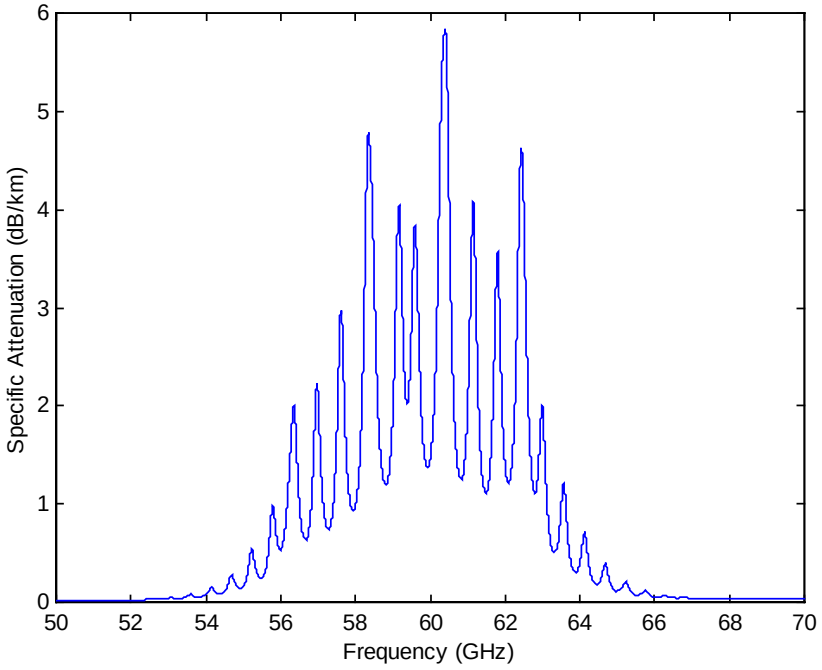

Figure 5.9 - Specific attenuation of atmospheric oxygen at a pressure of 75 mbar and an altitude of 18 km (59,400 ft) based on a standard atmosphere.

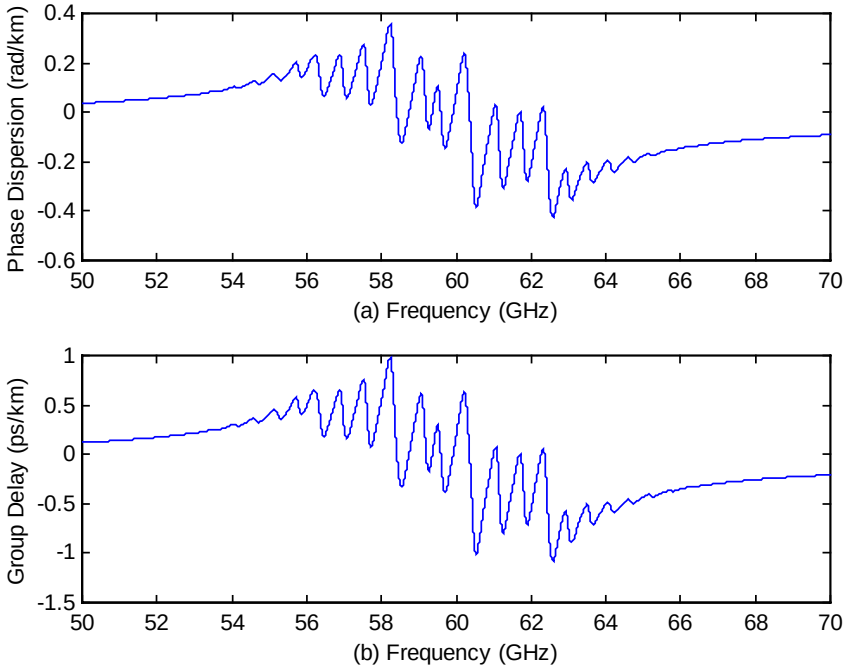

Figure 5.10 - Phase dispersion (a) and group delay (b) of atmospheric oxygen at P = 75 mbar.

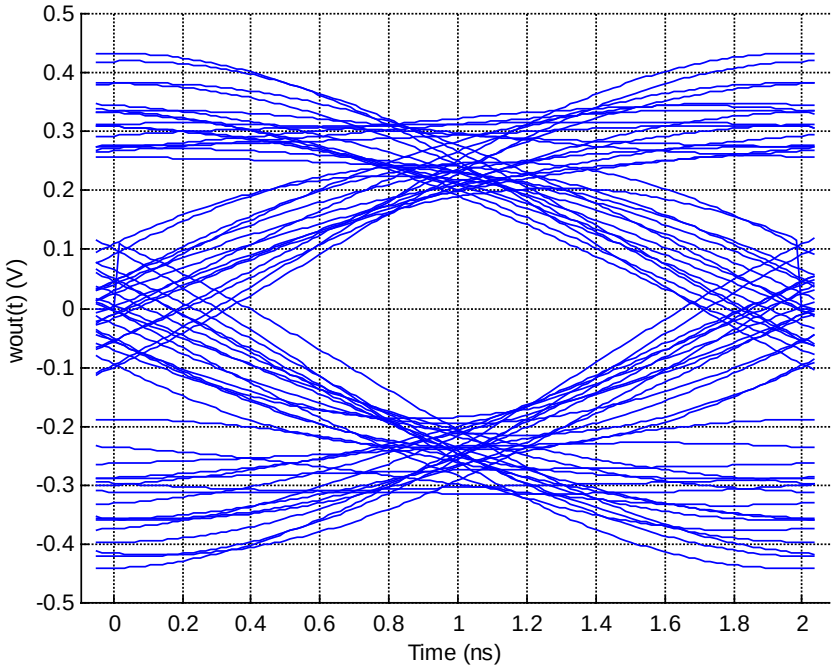

Figure 5.11 - Eye diagram with atmospheric oxygen present in the link with P = 75 mbar, R_b = 0.5 Gbps, and d = 1 km.

5.3 Variable – Data Rate

All of the simulations until now use a data rate of R_b = 500 Mbps. As the data rate increases, the effect of phase dispersion and group delay in the signal becomes more noticeable. In this section, the eye diagrams for data rates of R_b = 1 Gbps and R_b = 2 Gbps are examined, where the distance and frequency range of the link are 1 km and 50 GHz to 70 GHz, respectively. Eye diagrams for each data rate are presented for the following conditions: atmospheric oxygen is not present in the link; atmospheric oxygen is present with a pressure of 1013 mbar; atmospheric oxygen is present with a pressure of 310 mbar; and atmospheric oxygen is present with a pressure of 75 mbar.

5.3.1 1 Gbps

The eye diagrams for P = 1013 mbar, P = 310 mbar, and P = 75 mbar are separately compared to the eye diagram without atmospheric oxygen in the link. The structure of the eye diagrams in Figure 5.13 and Figure 5.14 is similar to the structure of the diagram in Figure 5.12, where the center peak voltage is V_{center} = ~0.20 V and the center of the eye is Δt = 0.6 ns. In all three of these figures, spreading in the signal is noticeable, but it is minimized in Figure 5.14. The differences between the eye diagrams at R_b = 1 Gbps is more noticeable than in the eye diagrams at R_b = 500 Mbps.

In Figure 5.15, the structure of the eye diagram is more defined than what is seen in Figure 5.14. In this case, the peak center voltage is V_{center} = ~ 0.17 V and the width of the eye is Δt = 0.7 ns. At this pressure, the atmospheric oxygen absorption clearly alters the original waveform presented in Figure 5.12.

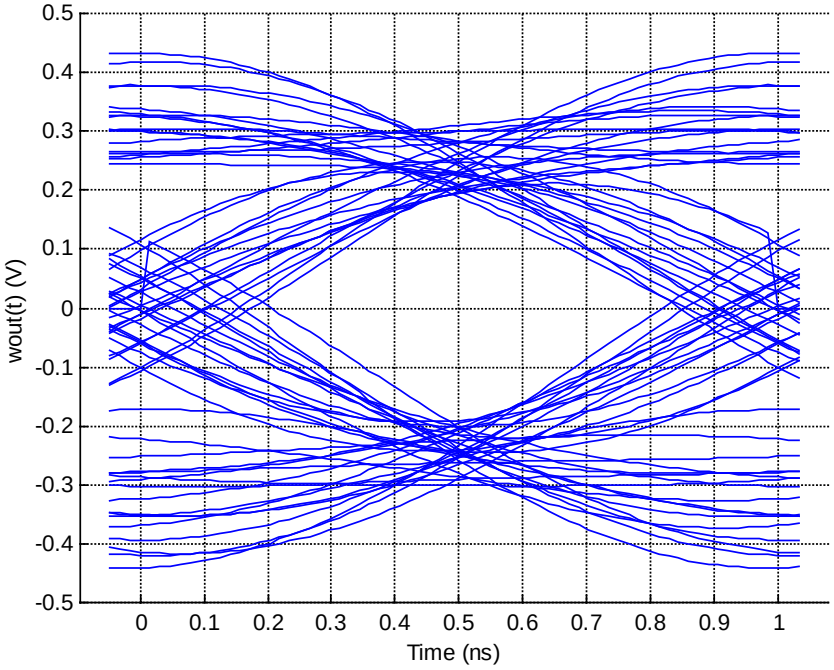

Figure 5.12 - Eye diagram without atmospheric oxygen present in the link.

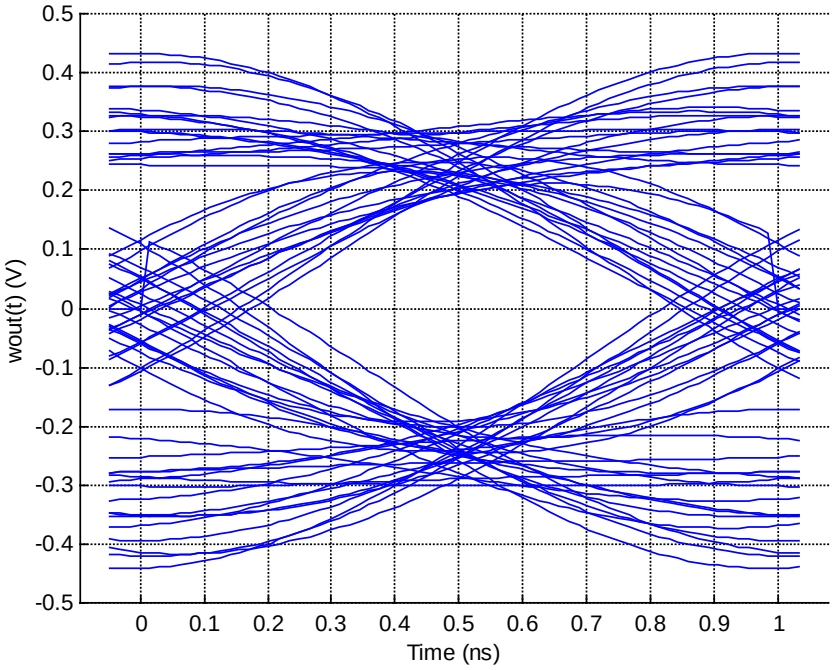

Figure 5.13 - Eye diagram with atmospheric oxygen present in the link with P = 1013 mbar, R_b = 1.0 Gbps, and d = 1 km.

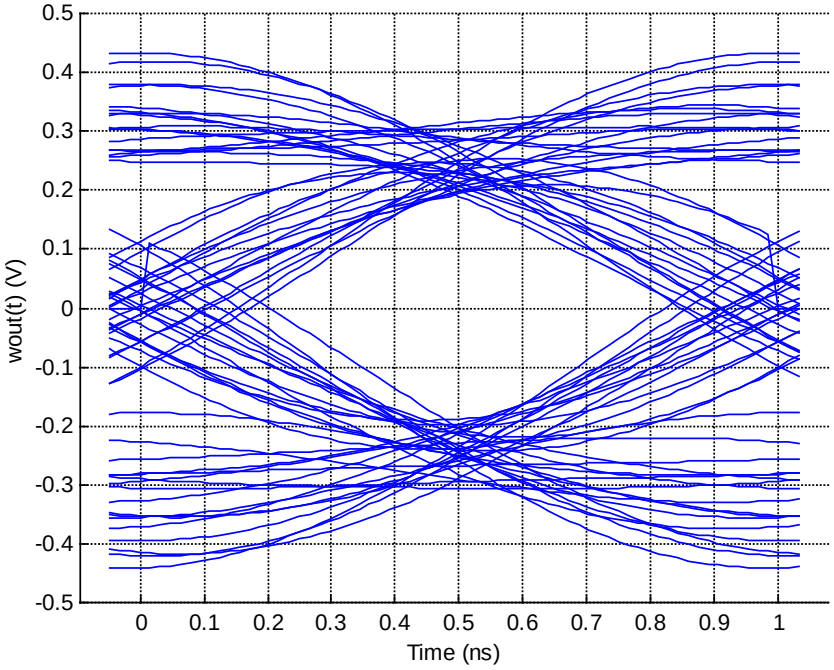

Figure 5.14 - Eye diagram with atmospheric oxygen present in the link with P = 310 mbar, R_b = 1.0 Gbps, and d = 1 km.

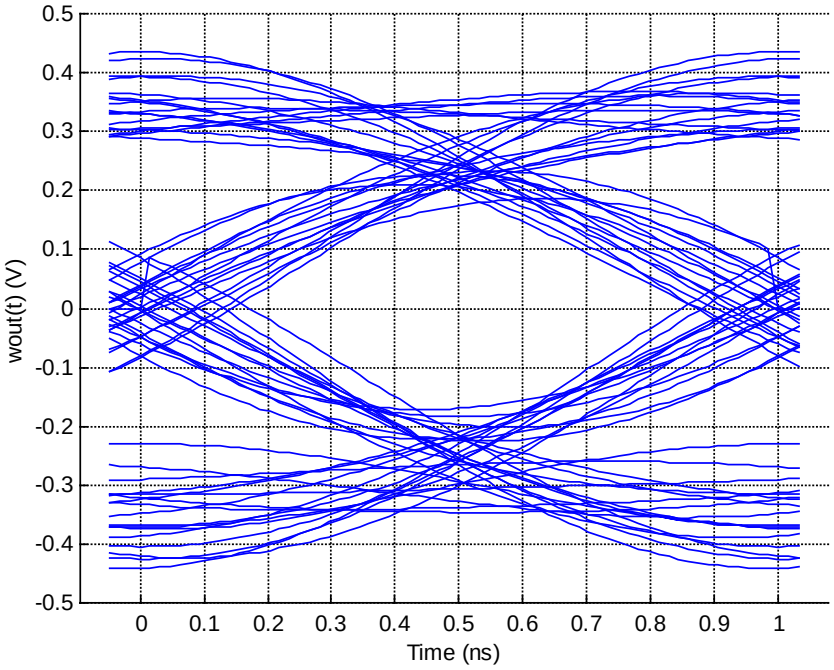

Figure 5.15 - Eye diagram with atmospheric oxygen present in the link with P = 75 mbar, R_b = 1.0 Gbps, and d = 1 km.

5.3.2 2 Gbps

The effect of atmospheric oxygen absorption in a digital link is greater for a data rate of R_b = 2 Gbps, than it is for a data rate of R_b = 500 Mbps. For R_b = 500 Mbps, the difference between the eye diagrams was difficult to distinguish. For R_b = 2 Gbps, the differences between eye diagrams, such as signal distortion, are obvious.

The structure of the eye diagrams and the distortion in the signal are distinguishable in Figure 5.16 and Figure 5.17. In both figures, the peak center voltage is V_{center} = ~ 0.19 V and the width is Δt = 0.3 ns.

For P = 310 mbar, the waveform appears distorted as compared to both the eye diagram with P = 1013 mbar and the eye diagram without atmospheric oxygen present. The center peak voltage is a little less (V_{center} ~ = 0.18 V) but the width is still Δt = 0.3 ns.

For P = 75 mbar, the atmospheric oxygen absorption distorts the waveform presented in the eye diagram of Figure 5.19. At this pressure, the contributions from neighboring lines are small, which results in lower total attenuation. These lines also appear in the phase dispersion, resulting in the distortion of the waveform. The peak voltage in the center of the eye is reduced to V_{center} = ~ 0.15 V and the width of the eye is increased to Δt = 0.4 ns.

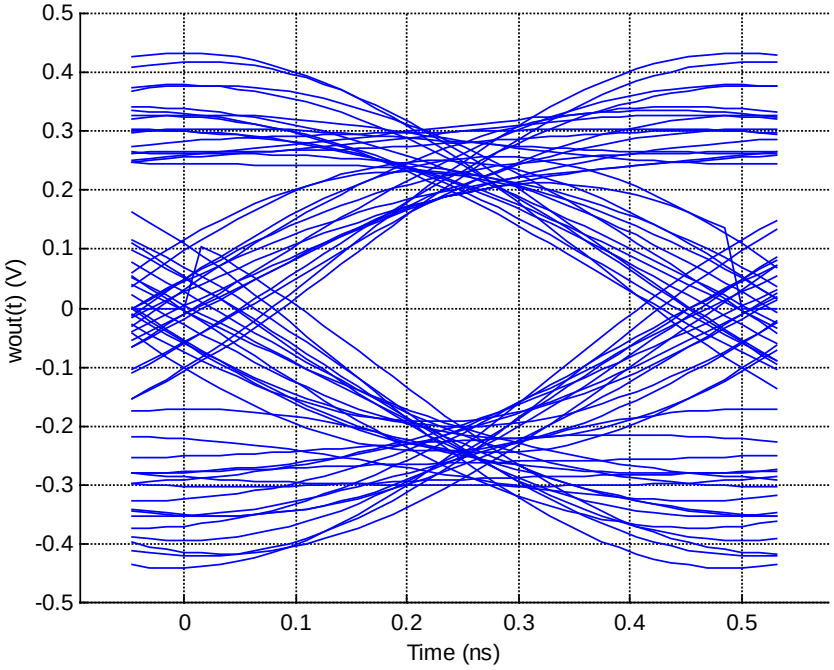

Figure 5.16 - Eye diagram without atmospheric oxygen present in the link.

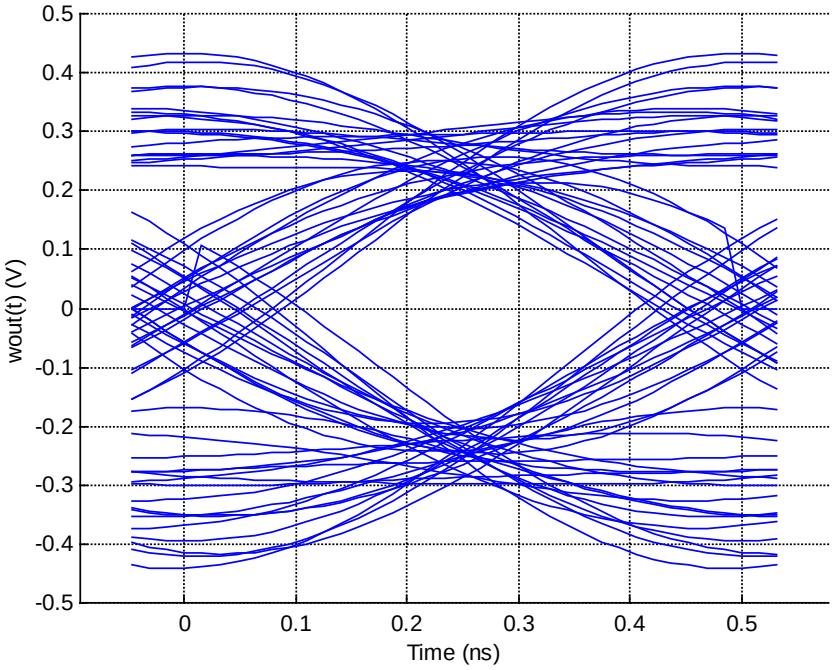

Figure 5.17- Eye Diagram with Atmospheric Oxygen Present in the Link with P = 1013 mbar, R_b = 2.0 Gbps, and d = 1 km.

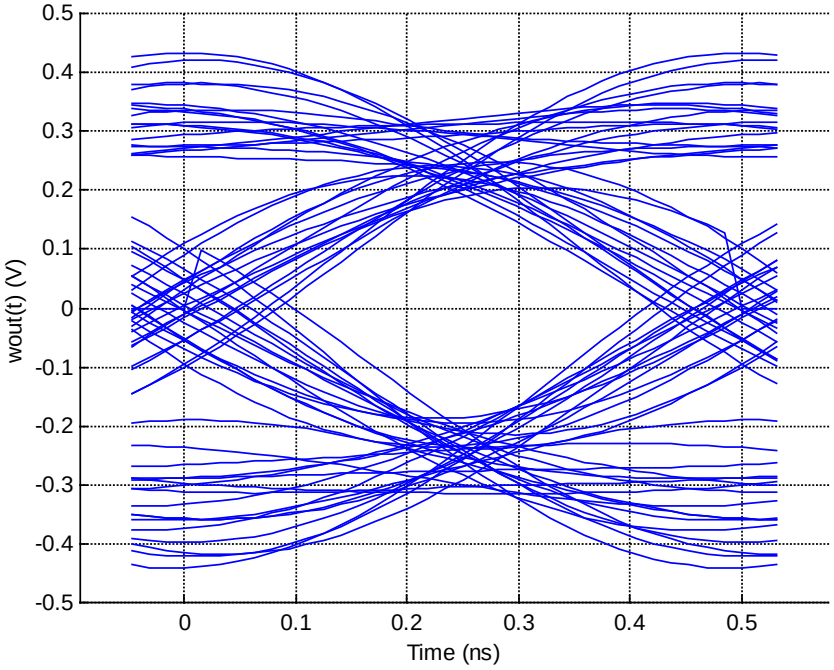

Figure 5.18- Eye Diagram with Atmospheric Oxygen Present in the Link with P = 310 mbar, R_b = 2.0 Gbps, and d = 1 km.

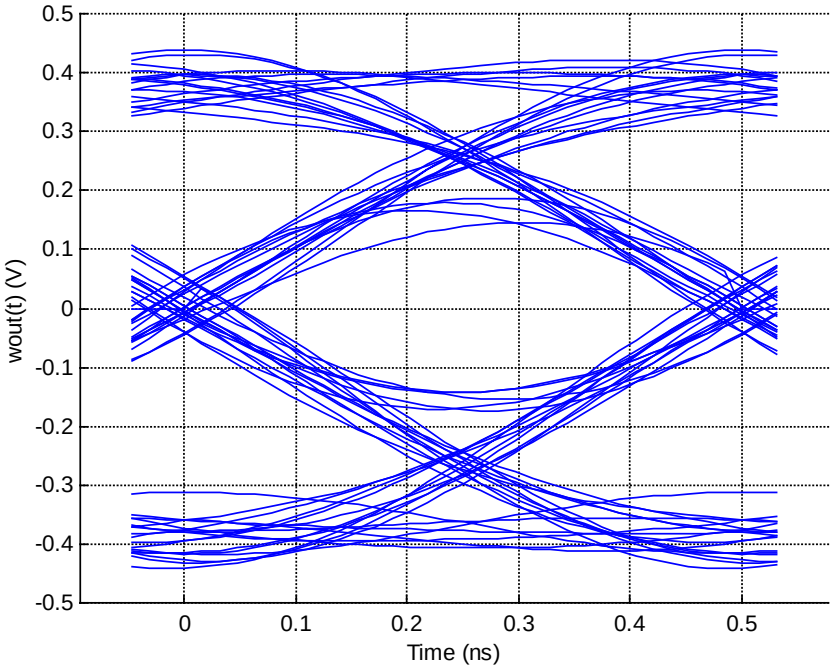

Figure 5.19 - Eye Diagram with Atmospheric Oxygen Present in the Link with P = 75 mbar, R_b = 2.0 Gbps, and d = 1 km.

5.4 Bit Error Rate (BER) Plots

The effects of atmospheric oxygen are seen in the BER plots. In Figure 5.20, the probability of bit error, P_e, is plotted against the carrier to noise ratio in dB. The dispersion due to oxygen has more of an impact on a wideband signal at lower atmospheric pressures than at higher pressures. At lower pressures, an increase in data rate requires more margin in order to meet the minimum carrier to noise ratio (C/N) as seen in Figure 5.20. The lines corresponding to P = 310 mbar and P = 1013 mbar are close to the line that corresponds to the link without oxygen present. The blue line in Figure 5.20 corresponds to the BER curve for R_b = 2.0 Gbps at P = 75 mbar. At P = 75 mbar, R_b = 2.0 Gbps, and $P_e = 10^{-6}$, an additional margin of 2.5 dB/km is required for the required C/N. At Rb = 0.5 Gbps, the margin required is small (< 0.1 dB/km) for the atmospheric pressures of 75 mbar, 310 mbar, and 1013 mbar, as seen in Figure 5.21. For Rb = 1.0 Gbps, the margin required increases to 1 dB/km for an atmospheric pressure of 75 mbar and is less than 0.1 dB/km for a pressure of 310 mbar and 1013 mbar.

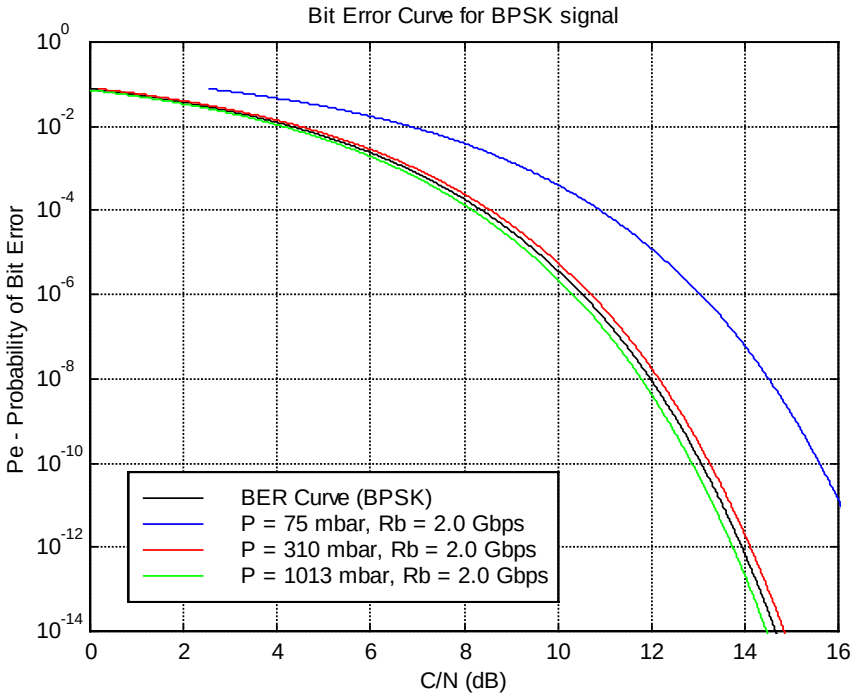

Figure 5.20 – BER plots for R_b = 2.0 Gbps at different atmospheric pressures.

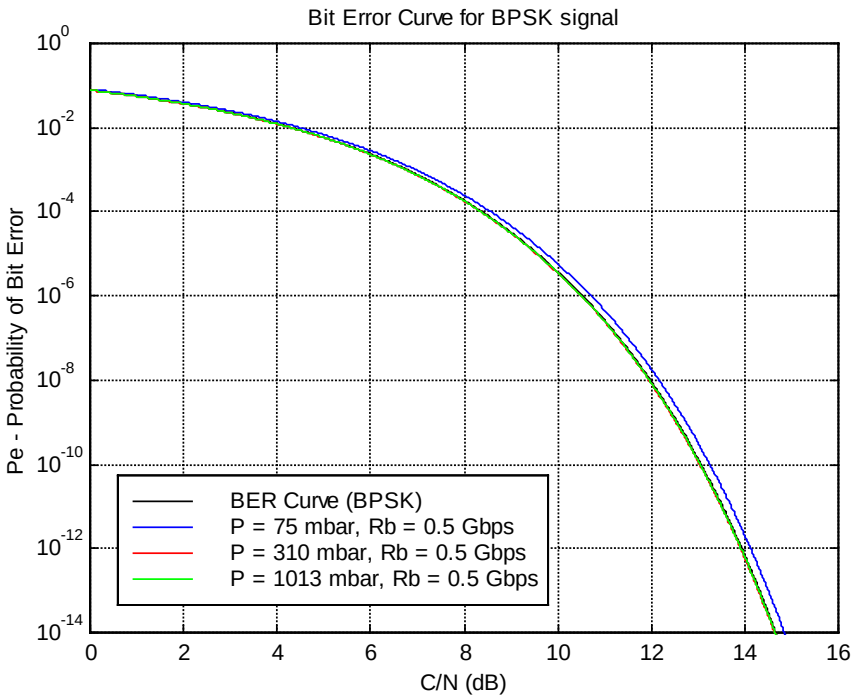

Figure 5.21 - BER plots for R_b = 0.5 Gbps at different atmospheric pressures.

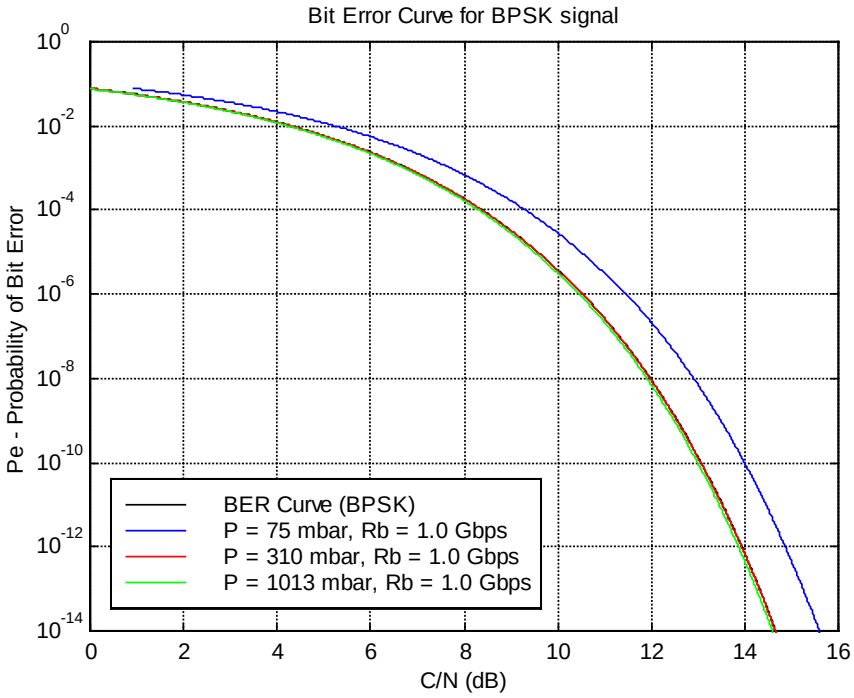

Figure 5.22 - BER plots for R_b = 1.0 Gbps at different atmospheric pressures.

Chapter 6 - Conclusion

A summary of the thesis, a summary of the results, and suggestions for future work are presented in the following sections. The background for the properties of atmospheric oxygen, the atmospheric model, and the simulation of the communication system are summarized in Section 6.1. The results summary includes a discussion on what was achieved in running the simulations. Suggestions for future work are given in Section 6.3.

6.1 Thesis Summary

Atmospheric oxygen attenuates the energy and distorts the phase of digital signals in the 60 GHz band. For low bandwidth signals, the impact of atmospheric oxygen in the link is very small, other than the high specific attenuation. For wideband signals, the presence of atmospheric oxygen in the link has more of an effect on the signal causing distortion of the signal waveform, leading to an increase in BER of digital links. Even though the impact of atmospheric oxygen in a wideband link is accounted for by allotting a margin in the link budget analysis, understanding why and how the attenuation and phase dispersion of the signal exist in the link is important, especially if the communication system is located at a significant altitude above sea level.

In Chapter 2, the physical behavior of atmospheric oxygen was first explained in order to understand how atmospheric oxygen absorbs electromagnetic waves. In short, atmospheric oxygen absorption is due to the interaction between its magnetic dipole moment and these waves. In addition, the structure of atmospheric oxygen consists of three closely spaced rotational states. Absorption occurs when atmospheric oxygen resonates, which is due to electrons transitioning between these states.

Besides discussing how atmospheric oxygen absorbs electromagnetic waves, equations were presented that characterize the absorption. The equations were also presented as the

foundation for the analysis presented in Chapter 3. These equations also describe how the absorption due to oxygen changes with atmospheric pressure. The plots describing the absorption due to atmospheric oxygen as a function of frequency change from being smooth and broad at P = 1013 mbar to a series of individual lines at P = 75 mbar.

The equations presented in Chapter 2 did not describe the phase dispersion due to atmospheric oxygen, which is important for examining the effects of atmospheric oxygen on a wideband signal. Instead of using these equations directly, an atmospheric model was used that included equations to simulate the phase dispersion due to atmospheric oxygen. The atmospheric model in Chapter 3 included equations that simulated the contributions from neighboring resonant frequency lines and from the nonresonant part of the oxygen molecule. In order to represent atmospheric oxygen absorption in the link, the specific attenuation and phase dispersion were represented collectively in a transfer function.

A computer program was written to simulate a communication system with atmospheric oxygen in the link, which is discussed in Chapter 4. A block diagram of the communication system was presented in order to visualize the simulation process. Chapter 4 includes explanations of how each of the blocks in the communication system, including the atmosphere, was simulated. Appendix A provides a review of the simulator and includes test results.

6.2 Results Summary

The results presented in Chapter 5 reveal the effects of atmospheric oxygen on a wideband digital link. Eye diagrams, obtained at the receive end of the simulated link, were used to study the effect of molecular oxygen as a wideband BPSK link at 60 GHz.

As the pressure decreases, the appearance of individual resonance lines in the attenuation and dispersion curves becomes more discernible. At lower atmospheric pressures, the widths of individual resonance lines are minimized, contributing less total attenuation but increasing the effects of phase dispersion in the signal. The structure of the eye in the eye diagrams is more defined with a decrease in pressure. The results include attenuation, phase dispersion, and group delay plots for atmospheric pressures of 1013 mbar, 310 mbar, and 75 mbar. These results are compared against a signal without the presence of atmospheric oxygen in the link.

The results include data for data rates of 500 Mbps, 1 Gbps, and 2 Gbps. As the data rate increases, the atmospheric oxygen absorption has a greater impact on the signal, giving more distortion of received pulses which show up as changes in the eye diagram structure.

6.3 Future Work

The research for understanding and characterizing the effects of atmospheric oxygen on wideband digital signals is in its early stages. Although this thesis examines the effects of atmospheric oxygen absorption on a wideband signal in the 60 GHz band, avenues for research still exist.

1. The communication system simulated in this thesis used BPSK modulation. The communication system should be simulated with other multi-level modulation schemes, such as QPSK, 16-QAM, and 256-QAM. In these systems, the effect of atmospheric oxygen absorption could be enough to alter the waveform such that the information sent is decoded incorrectly, resulting in bit errors in the received signal.
2. The simulation discussed in Chapter 4 only included the effects due to dry air. The atmospheric model also includes equations to simulate the effects of water vapor, rain, and fog present in the atmosphere. As the wavelength of digital signals becomes smaller, obstructions have a larger impact on these signals. For outdoor links, atmospheric conditions, such as rain, determine if a link is feasible.
3. The simulation discussed in Chapter 4 considered only horizontal links and did not examine the effects of the atmosphere on a slant path to a satellite. Since a signal at 60 GHz cannot penetrate the earth's atmosphere, it is interesting to see at what altitudes and elevation angles the signal can and cannot be received.
4. One suggestion for compensating for the effects of atmospheric oxygen absorption in the link is to allot a bigger margin in the link budget. Another suggestion is to devise passive and active equalizers to correct the dispersive effects due to atmospheric oxygen. The research for equalizers requires an understanding of the physical properties of the atmosphere due to atmospheric oxygen and how to compensate for these properties at various atmospheric pressures.

Appendix A

Here is a copy of the code used for the simulation of a BPSK communication system, which includes the code for the atmospheric model.

```
%%%%%%%%%%%%%%%%%%%%%%%%%%%%%%%%%%%%%%%%%%%%%%%%%%%%%%%%%%%%%%%%%%%%%%%%%%%%%%%
%%%                                                                       %%%
%%%   Name: Adelia Valdez                                                 %%%
%%%                                                                       %%%
%%%   Date: April 7, 2001                                                 %%%
%%%                                                                       %%%
%%%   Title: BPSK Simulation including the Atmospheric Model              %%%
%%%                                                                       %%%
%%%   Description: This simulation includes the modeling of a simple     %%%
%%%        BSPK communication system, where the atmospheric               %%%
%%%        absorption and dispersion due to oxygen are included           %%%
%%%        in the link.                                                   %%%
%%%                                                                       %%%
%%%%%%%%%%%%%%%%%%%%%%%%%%%%%%%%%%%%%%%%%%%%%%%%%%%%%%%%%%%%%%%%%%%%%%%%%%%%%%%

close all;
clear all;

%%%%%%%%%%%%%%%%%%%%%%%%%%%%%%%%%%%%%%%%%%%%%%%%%%%%%%%%%%%%%%%%%%%%%%%%%%%%%%%%%
%%%                                                                       %%%
%%%   This program begins with establishing a bit sequence of 1s and 0s,      %%%
%%%   which is then converted to +1 and -1 voltage levels.  After         %%%
%%%   converting the bits to +/- 1 V, the sequence is then modulated using    %%%
%%%   BPSK.                                                               %%%
%%%                                                                       %%%
%%%%%%%%%%%%%%%%%%%%%%%%%%%%%%%%%%%%%%%%%%%%%%%%%%%%%%%%%%%%%%%%%%%%%%%%%%%%%%%%%

%%%%%%%%%%%%%%%%%%%%%%%%%%%%%%%%%%%%%%%%%%%%%%%%%%%%%%%%%%%%%%%%%%%%%%%%%%%%%%%%%
%%%                                                                       %%%
%%%   SYSTEM PARAMETERS                                                       %%%
%%%                                                                       %%%
%%%   Note: Symbol rate equals bit rate for BPSK                          %%%
%%%                                                                       %%%
%%%   Since this program takes some time to run, every effort was made    %%%
%%%   to speed up the program, which is seen in generating the BPSK           %%%
%%%   signal.  The generated spectrum of the BPSK signal is centered      %%%
%%%   around a frequency which is a power of two.  The spectrum is        %%%
%%%   then shifted in the frequency domain to the carrier frequency.      %%%
%%%                                                                       %%%
%%%%%%%%%%%%%%%%%%%%%%%%%%%%%%%%%%%%%%%%%%%%%%%%%%%%%%%%%%%%%%%%%%%%%%%%%%%%%%%%%

m = 6;                 % Power of two
N = 2^m;                % Number of symbols
```

```
Rb = 2;               % (Gbps) Bit Rate
Ts = 1/Rb;            % (ns)   Symbol Period
r = 0.25;             % Roll-off factor for filters
dt = 1/(N);           % Increment of time
fc = 16;              % (GHz)  Carrier Frequency
wc = 2 * pi * fc;     % (Grad/s)
dist = 1;              % (km) - Path Length

%%%%%%%%%%%%%%%%%%%%%%%%%%%%%%%%%%%%%%%%%%%%%%%%%%%%%%%%%%%%%%%%%%%%%%%%%%%%%%%
%%%                                                                          %%%
%%%   BIT GENERATOR                                                          %%%
%%%                                                                          %%%
%%%   Generates N symbols, where the symbol period of each symbol is Ts.     %%%
%%%   In this case, a symbol is either a 1 or 0.                             %%%
%%%                                                                          %%%
%%%%%%%%%%%%%%%%%%%%%%%%%%%%%%%%%%%%%%%%%%%%%%%%%%%%%%%%%%%%%%%%%%%%%%%%%%%%%%%

% BIT GENERATOR: Generate a random vector of 1s and 0s.
n = 1:N;                          % Number of symbols generated
nz = size(n);                     % Size of n
rand = mod(randperm(nz(2)),2);    % Generates a vector of random 1s and 0s
t = zeros(1,Ts/dt+1);             % Initializes the 't' vector
tsym = zeros(1,Ts*nz(2)/dt+1);    % Initializes the 'tsym' vector
win = zeros(1,Ts*nz(2)/dt+1);     % Initializes the 'win' vector

for j = 1:nz(2)
   t = (j-1)*Ts:dt:j*Ts-dt;       % Time vector for each symbol
   tz = size(t);                  % Size of the time vector

   for i = 1:tz(2)
        x(i) = rand(j);           % Generates a digital signal
                                  % Holds the voltage level for one symbol
                                  % period
   end

   if j == 1
      tsym = t;                   % Generates the time vector
      win = x;                    % Generates the 'win(t)' signal
   else
      tsym = [tsym t];
      win = [win x];
   end
end

%%%%%%%%%%%%%%%%%%%%%%%%%%%%%%%%%%%%%%%%%%%%%%%%%%%%%%%%%%%%%%%%%%%%%%%%%%%%%%%
%%%                                                                          %%%
%%%   VOLTAGE CONVERTER                                                          %%%
%%%                                                                          %%%
%%%   Converts the voltage level from 0 V and 1V to -1 V and +1 V,           %%%
%%%   respectively.                                                          %%%
%%%                                                                          %%%
%%%%%%%%%%%%%%%%%%%%%%%%%%%%%%%%%%%%%%%%%%%%%%%%%%%%%%%%%%%%%%%%%%%%%%%%%%%%%%%

mt = (-1).^(win-1);

%%%%%%%%%%%%%%%%%%%%%%%%%%%%%%%%%%%%%%%%%%%%%%%%%%%%%%%%%%%%%%%%%%%%%%%%%%%%%%%
%%%                                                                          %%%
%%%   BPSK MODULATOR                                                         %%%
%%%                                                                          %%%
%%%   Modulates the signal, m(t), using BPSK.  See 'Digital and Analog       %%%
%%%   Communication Systems' by Leon Couch for background.  See equation     %%%
%%%   (5-77) on page 343 in the 6th ed.                                      %%%
%%%                                                                          %%%
```

```
%%%   Note: The variable 'o' will be used for numbering the figures.          %%%
%%%         The variable is incremented before each figure.                  %%%
%%%                                                                          %%%
%%%%%%%%%%%%%%%%%%%%%%%%%%%%%%%%%%%%%%%%%%%%%%%%%%%%%%%%%%%%%%%%%%%%%%%%%%%%%%%

Ac = 1;                                         % Amplitude of modulated signal
stin = -Ac .*mt .* sin(wc .* tsym);             % BPSK modulated signal

o = 1;                                          % Initialize the variable 'o'
figure(o)                                       % This figure contains the plots
subplot(311)                                    % of the the generated bit sequence,
plot(tsym,win)                                  % the converted sequence, and the
xlabel('Time (ns)'), ylabel('win(t)')           % BPSK modulated signal.
title('TX - Digital Input Signal')
axis([-0.1 nz(2)*Ts+.1 -0.1 1.1])
subplot(312)
plot(tsym,mt)
xlabel('Time (ns)'), ylabel('m(t)')
title('TX - NRZ Signal')
axis([-0.2 max(tsym)+.2 -1.2 1.2])
subplot(313)
plot(tsym,stin)
xlabel('Time (ns)'), ylabel('sin(t)')
title('TX - BPSK Modulated Signal')
axis([-0.1 max(tsym)+.1 min(stin)-0.1 max(stin)+0.1])

%%%%%%%%%%%%%%%%%%%%%%%%%%%%%%%%%%%%%%%%%%%%%%%%%%%%%%%%%%%%%%%%%%%%%%%%%%%%%%%
%%%                                                                          %%%
%%%   FOURIER TRANSFORM - Time to Frequency                                  %%%
%%%                                                                          %%%
%%%%%%%%%%%%%%%%%%%%%%%%%%%%%%%%%%%%%%%%%%%%%%%%%%%%%%%%%%%%%%%%%%%%%%%%%%%%%%%

Sfin = fft(stin);                       % FFT of signal 'stin'
Sf = fftshift(Sfin);                % Shift and center the signal
fz = size(Sf);
f = linspace(-(N/2),(N/2),fz(2));

Sfmag = abs(Sf)./max(abs(Sf));    % Normalizing the spectrum to 1 for plotting
Sfpha = angle(Sf);                % Angle of Sf

o = o+1;
figure(o)
plot(f,Sfmag)
axis([min(f) max(f) min(Sfmag) max(Sfmag)])


%%%%%%%%%%%%%%%%%%%%%%%%%%%%%%%%%%%%%%%%%%%%%%%%%%%%%%%%%%%%%%%%%%%%%%%%%%%%%%%
%%%                                                                          %%%
%%%   ROOT RAISED COSINE FILTER - Transmitter     & EQUALIZER FILTER          %%%
%%%                                                                          %%%
%%%   Recall from above r = 0.25.                                            %%%
%%%                                                                          %%%
%%%   Note: See Couch page 183 in the 6th ed. for discussion of Nyquist      %%%
%%%         RRC filters.                                                     %%%
%%%                                                                          %%%
%%%%%%%%%%%%%%%%%%%%%%%%%%%%%%%%%%%%%%%%%%%%%%%%%%%%%%%%%%%%%%%%%%%%%%%%%%%%%%%

Bw = (Rb/2) * (1 + r);            % (GHz) - Signal Bandwidth
f1 = (Rb/2) * (1 - r);
fdelta = r*Rb/2;

Hef = zeros(1,fz(2));             % Initializes 'Hef' vector
Hq = zeros(1,fz(2));              % Initializes 'Hq' vector
```

```
for i = 1:fz(2)
     % Raised Cosine filter - centered on fc
     if (f(i) >= fc + Bw) & (f(i) <= fc - Bw)
          Hef(i) = 0;
     elseif (f(i) < fc + Bw) & (f(i) > fc + f1)
          Hef(i) = (1/2) * (1 + cos(pi * (f(i) - (fc + f1)) / (2 * fdelta)));
     elseif (f(i) <= fc + f1) & (f(i) >= fc - f1)
          Hef(i) = 1;
     elseif (f(i) <  fc - f1) & (f(i) > fc - Bw)
          Hef(i) = (1/2) * (1 + cos(pi * (f(i) - (fc-f1)) / (2 * fdelta)));
     end

     % Equalizer TF - centered on fc
     if (f(i) >= fc - Rb/(2)) & (f(i) <= fc + Rb/(2))
          Hq(i) = (pi*(f(i) - fc)*Ts)/sin(pi*(f(i) - fc)*Ts);
     else
          Hq(i) = 0;
     end
end

Ht = sqrt(Hef);                         % Root Raised Cosine Filter (Tx)
Trf = Sf .* Hq .* Ht;                   % Transmit Spectrum after RRC filter
Trfmag = abs(Trf)./max(abs(Sf));        % Normalizing the spectrum to 1 for plotting
Trfpha = angle(Trf);                     % Angle of Trf

o = o+1;
figure(o)
subplot(411)
plot(f,Sfmag)
xlabel('Frequency (GHz)'), ylabel('Sin(f)')
title('TX - Spectrum of BPSK Modulator')
axis([min(f)-0.05 max(f)+0.05 min(Sfmag) max(Sfmag)])
subplot(412)
plot(f,Hq)
xlabel('Frequency (GHz)'), ylabel('Hq(f)')
title('TX - Plot of Equalizer TF')
axis([min(f)-0.05 max(f)+0.05 min(Hq)-0.5 max(Hq)+0.5])
subplot(413)
plot(f,Ht)
xlabel('Frequency (GHz)'), ylabel('Ht(f)')
title('TX - TF of the RRC filter')
axis([min(f)-0.05 max(f)+0.05 min(Ht)-0.5 max(Ht)+0.5])
subplot(414)
plot(f,Trfmag)
xlabel('Frequency (GHz)'), ylabel('Tr(f)')
title('TX - Spectrum from RRC filter')
axis([min(f)-0.05 max(f)+0.05 min(Trfmag) max(Trfmag)])

%%%%%%%%%%%%%%%%%%%%%%%%%%%%%%%%%%%%%%%%%%%%%%%%%%%%%%%%%%%%%%%%%%%%%%%%%%%%%%%
%%%                                                                          %%%
%%%   O2 ATTENUATION                                                         %%%
%%%                                                                          %%%
%%%   This model is from Liebe's 1989 paper.                                 %%%
%%%   H. J. Liebe.  "MPM - An Atmospheric Millimeter-wave Propagation        %%%
%%%   Model."  International Journal of Infrared and Millimeter Waves.       %%%
%%%   10.6 (1989): 631-650.                                                  %%%
%%%                                                                          %%%
%%%   COMPLEX REFRACTIVITY MODEL                                             %%%
%%%   Nt(f) = No + N(f) = No + N'(f) - iN"(f)                                    %%%
%%%                                                                          %%%
%%%   EQUATIONS FOR ATMOSPHERIC ABSORPTION, DISPERSION, AND GROUP DELAY      %%%
%%%   alpha(f) = 0.1820 f N''(f)                                             %%%
```

```
%%%   beta(f) = 1.2008 f N'(f)                                          %%%
%%%   tau = 3.336 N'(f)                                                     %%%
%%%                                                                     %%%
%%%%%%%%%%%%%%%%%%%%%%%%%%%%%%%%%%%%%%%%%%%%%%%%%%%%%%%%%%%%%%%%%%%%%%%%%%%

%%%%%%%%%%%%%%%%%%%%%%%%%%%%%%%%%%%%%%%%%%%%%%%%%%%%%%%%%%%%%%%%%%%%%%%%%%%
%%%                                                                     %%%
%%%   INITIAL PARAMETERS    & ATMOSPHERIC CONDITIONS                    %%%
%%%                                                                     %%%
%%%   Pressure and temperature based on standard atmosphere.            %%%
%%%                                                                     %%%
%%%%%%%%%%%%%%%%%%%%%%%%%%%%%%%%%%%%%%%%%%%%%%%%%%%%%%%%%%%%%%%%%%%%%%%%%%%

P = 1013;                   % (mbar) - Atmospheric Pressure based
T = (15)+273.15;            % (Kelvins) - Temperature
U = 0.05;                   % (%) - Relative Humidity; 5% for dry air

theta = 300/(T);            % Relative inverse temperature
v = 1.0;                    % g/m^3; Vapor Concentration
e = v/(7.223*theta);        % kPa; partial pressure for water vapor
p = P-e;                    % kPa; partial pressure for dry air

%%%%%%%%%%%%%%%%%%%%%%%%%%%%%%%%%%%%%%%%%%%%%%%%%%%%%%%%%%%%%%%%%%%%%%%%%%%
%%%                                                                     %%%
%%%   NONDISPERSIVE REFRACTIVITY                                        %%%
%%%                                                                     %%%
%%%   No = N1                                                           %%%
%%%                                                                     %%%
%%%%%%%%%%%%%%%%%%%%%%%%%%%%%%%%%%%%%%%%%%%%%%%%%%%%%%%%%%%%%%%%%%%%%%%%%%%

N1 = 2.588.*p*theta;        % Dry Air
No = N1;                    % Nondispersive Refract.

%%%%%%%%%%%%%%%%%%%%%%%%%%%%%%%%%%%%%%%%%%%%%%%%%%%%%%%%%%%%%%%%%%%%%%%%%%%
%%%                                                                     %%%
%%%   DISPERSIVE COMPLEX REFRACTIVITY                                   %%%
%%%                                                                     %%%
%%%   N = (Nl + Nd), where                                              %%%
%%%   Nl is the moist air resonance contributions,                      %%%
%%%   and Nd is the dry air nonresonant spectra.                        %%%
%%%                                                                     %%%
%%%%%%%%%%%%%%%%%%%%%%%%%%%%%%%%%%%%%%%%%%%%%%%%%%%%%%%%%%%%%%%%%%%%%%%%%%%

% Nl - Local Line Absorption and Dispersion
% Spectroscopic Parameters
a1 = load('a1.dat');             % kHz/mbar
a2 = load('a2.dat');             %
a3 = load('a3.dat');             % GHz/mbar
a4 = load('a4.dat');             %
a5 = load('a5.dat');             % 1/mbar
a6 = load('a6.dat');             % 1/mbar
fo = load('fo.dat');        % GHz - Line center frequencies
asz = size(fo);             % Size of table variables
fo2 = f+44;                 % GHz - Frequency range in the RF

% Line Parameters
S = a1*1e-7*p*theta^3.*exp(a2*(1-theta));              % (kHz) - Line Strength
gamma = a3*1e-4.*(p*theta.^(0.8-a4)+1.1*e*theta);      % (GHz) - Pressure-broadened
width
delta = (a5+a6*theta)*1e-4.*p*theta^0.8;               % Pressure Induced Interference

F1 = zeros(asz(1),fz(2));                              % Initializing vectors
F2 = zeros(asz(1),fz(2));
```

```
Nli1 = zeros(asz(1),fz(2));
Nli2 = zeros(asz(1),fz(2));
A = zeros(asz(1),fz(2));
B = zeros(asz(1),fz(2));
X = zeros(asz(1),fz(2));
Y = zeros(asz(1),fz(2));

for i = 1:fz(2)
     for j = 1:asz(1)
          % Abbreviations for the Complex Shape Function
          A(j,i) = gamma(j)*fo2(i)/fo(j);
          B(j,i) = (fo(j)^2 + gamma(j)^2)/fo(j);
          X(j,i) = (fo(j)-fo2(i))^2 + gamma(j)^2;
          Y(j,i) = (fo(j)+fo2(i))^2 + gamma(j)^2;

          % Shape Function for Absorption
          F2(j,i) = A(j,i)/X(j,i) + A(j,i)/Y(j,i) - delta(j)*(fo2(i)/fo(j))*((fo(j)-
fo2(i))/X(j,i) + (fo(j)+fo2(i))/Y(j,i));
          % Shape Function for Dispersion
          F1(j,i) = (B(j,i)-fo2(i))/X(j,i) + (B(j,i)+fo2(i))/Y(j,i) - 2/fo(j) +
delta(j)*(A(j,i)/X(j,i) - A(j,i)/Y(j,i));

          % Local-Line Resonance Contributions
          Nli1(j,i) = S(j) * F1(j,i);
          Nli2(j,i) = S(j) * F2(j,i);
     end
end

Nli1 = cumsum(Nli1,1);        % Moist Air Resonance Contributions
Nli2 = cumsum(Nli2,1);        % Moist Air Resonance Contributions

Nl1 = Nli1(asz(1),:);
Nl2 = Nli2(asz(1),:);

% Nd - Nonresonant Dry Air Spectrum
Sd = 6.14e-5*p*theta^2;                 % Debye Strength
gammao = 5.6e-4*(p+1.1*e)*theta;        % Debye Width
ap = 1.40.*(1-1.2e-5.*fo2.^1.5)*1e-10;  % Contribution from N2 absorption

Nd2 = Sd.*fo2/gammao.*(1+(fo2/gammao).^2).^-1+ap.*fo2*p^2*theta^3.5;
Nd1 = Sd.*(1./(1+(fo2/gammao).^2)-1);

% Complex Refractivity Model
Nt2 = Nl2 + Nd2;
Nt1 = Nl1 + Nd1;

alphadB = 0.1820.*fo2.*Nt2;
beta = 1.2008.*fo2.*Nt1;
betadeg = beta*(pi/180);
tau = 3.336.*(Nt1);

% Customizing the title for the absorption and dispersion plots
Pres = num2str(P);
Dist = num2str(dist);
tit1 = ['LINK - Specific Attenuation of Oxygen at ' Pres ' mbar' ];
tit2 = ['(a) LINK - Phase Dispersion of Oxygen at ' Pres ' mbar'];
tit3 = ['(b) LINK - Group Delay of Oxygen at ' Pres ' mbar'];

o = o + 1;
figure(o)
plot(fo2, alphadB)
xlabel('Frequency (GHz)'), ylabel('Specific Attenuation (dB/km)')
axis([min(fo2) max(fo2) min(alphadB) max(alphadB)])
```

```
title(tit1)

o = o + 1;
figure(o)
subplot(211)
plot(fo2,betadeg)
xlabel('(a) Frequency (GHz)'), ylabel('Phase Dispersion (rad/km)')
title(tit2)
axis([min(fo2) max(fo2) min(betadeg) max(betadeg)])
subplot(212)
plot(fo2,tau)
xlabel('(b) Frequency (GHz)'), ylabel('Group Delay (ps/km)')
title(tit3)
axis([min(fo2) max(fo2) min(tau) max(tau)])

%%%%%%%%%%%%%%%%%%%%%%%%%%%%%%%%%%%%%%%%%%%%%%%%%%%%%%%%%%%%%%%%%%%%%%%%%%%%%%%
%%%                                                                          %%%
%%%   ATMOSPHERIC OXYGEN TRANSFER FUNCTION                                   %%%
%%%                                                                          %%%
%%%%%%%%%%%%%%%%%%%%%%%%%%%%%%%%%%%%%%%%%%%%%%%%%%%%%%%%%%%%%%%%%%%%%%%%%%%%%%%

c = 3e8;                                % Speed of light
k = 2*pi.*fo2/c;                        % Free space wave number
alpha = 10.^(-alphadB*dist/10);         % Converting alpha from dB into decimal
Atmo = alpha.*exp(i*beta.*k*dist);           % Atmospheric Oxygen Transfer Function

%%%%%%%%%%%%%%%%%%%%%%%%%%%%%%%%%%%%%%%%%%%%%%%%%%%%%%%%%%%%%%%%%%%%%%%%%%%%%%%
%%%                                                                          %%%
%%%   RECEIVED SPECTRUM                                                          %%%
%%%                                                                          %%%
%%%   Note: Throughout the rest of the program, a 'nc' is attached to a      %%%
%%%         variable, or vector if it did not have the atmosphere TF             %%%
%%%         inserted into the calculations                                   %%%
%%%                                                                          %%%
%%%%%%%%%%%%%%%%%%%%%%%%%%%%%%%%%%%%%%%%%%%%%%%%%%%%%%%%%%%%%%%%%%%%%%%%%%%%%%%

Rrf = Trf ./ Atmo;                      % Input Spectrum to the receiver w the
atmosphere
Rrfnc = Trf;                            % Input Spectrum to the receiver w/o the
atmosphere

Rrfmag = abs(Rrf)./max(abs(Sf));        % Normalizing the spectrum to 1 for plotting
Rrfpha = angle(Rrf);                     % Angle of Rrf
Rrfmagnc = abs(Rrfnc)./max(abs(Sf));     % Normalizing the spectrum to 1 for plotting
Rrfphanc = angle(Rrfnc);                 % Angle of Rrfnc

%%%%%%%%%%%%%%%%%%%%%%%%%%%%%%%%%%%%%%%%%%%%%%%%%%%%%%%%%%%%%%%%%%%%%%%%%%%%%%%
%%%                                                                          %%%
%%%   ROOT RAISED COSINE FILTER - Receiver                                   %%%
%%%                                                                          %%%
%%%   Recall from above r = 0.25.                                            %%%
%%%                                                                          %%%
%%%%%%%%%%%%%%%%%%%%%%%%%%%%%%%%%%%%%%%%%%%%%%%%%%%%%%%%%%%%%%%%%%%%%%%%%%%%%%%

Hr = sqrt(Hef);                         % Root Raised Cosine Filter (Rx)
Sfout = Rrf .* Hr;                       % Output Spectrum of Rx RRC filter
Sfoutnc = Rrfnc .* Hr;                   % Output Spectrum of Rx RRC filter

Sfomag = abs(Sfout)./max(abs(Sf));       % Normalizing spectrum for plot
Sfopha = angle(Sfout);                   % Scaling in terms of pi for plotting
Sfomagnc = abs(Sfoutnc)./max(abs(Sf));   % Normalizing spectrum for plot
Sfophanc = angle(Sfoutnc);               % Scaling in terms of pi for plotting
```

```
o = o+1;
figure(o)
subplot(311)
plot(f,Rrfmag)
xlabel('Frequency (GHz)'), ylabel('Rr(f)')
title('RX - Spectrum before RRC filter')
axis([min(f)-0.05 max(f)+0.05 min(Rrfmag) max(Rrfmag)])
subplot(312)
plot(f,Hr)
xlabel('Frequency (GHz)'), ylabel('Hr(f)')
title('RX - TF of the RRC filter')
axis([min(f)-0.05 max(f)+0.05 min(Hr) max(Hr)])
subplot(313)
plot(f,Sfomag)
title('RX - Output Spectrum of RRC filter')
xlabel('Frequency (GHz)'), ylabel('Sout(f)')
axis([min(f)-0.05 max(f)+0.05 min(Sfomag) max(Sfomag)])

%%%%%%%%%%%%%%%%%%%%%%%%%%%%%%%%%%%%%%%%%%%%%%%%%%%%%%%%%%%%%%%%%%%%%%%%%%%%%%%
%%%                                                                          %%%
%%%   INVERSE FOURIER TRANSFORM - Frequency to Time                          %%%
%%%                                                                          %%%
%%%%%%%%%%%%%%%%%%%%%%%%%%%%%%%%%%%%%%%%%%%%%%%%%%%%%%%%%%%%%%%%%%%%%%%%%%%%%%%

sfout = ifftshift(Sfout);              % Spectrum is shifted
sfoutnc = ifftshift(Sfoutnc);          % Inverse Fourier Transform
stout = ifft(sfout);                   % Spectrum is shifted
stoutnc = ifft(sfoutnc);               % Inverse Fourier Transform

%%%%%%%%%%%%%%%%%%%%%%%%%%%%%%%%%%%%%%%%%%%%%%%%%%%%%%%%%%%%%%%%%%%%%%%%%%%%%%%
%%%                                                                          %%%
%%%   BPSK DEMODULATOR                                                       %%%
%%%                                                                          %%%
%%%   Demodulates the BPSK signal.  See 'Digital and Analog Communication    %%%
%%%   Systems' by Leon Couch for background.  See equation (5-77) on         %%%
%%%   page 343 in the 6th ed.                                                %%%
%%%                                                                          %%%
%%%%%%%%%%%%%%%%%%%%%%%%%%%%%%%%%%%%%%%%%%%%%%%%%%%%%%%%%%%%%%%%%%%%%%%%%%%%%%%

rt = -Ac .* stout .* sin(wc .* tsym);        % BPSK demodulated signal
rtnc = -Ac .* stoutnc .* sin(wc .* tsym);    % BPSK demodulated signal

%%%%%%%%%%%%%%%%%%%%%%%%%%%%%%%%%%%%%%%%%%%%%%%%%%%%%%%%%%%%%%%%%%%%%%%%%%%%%%%
%%%                                                                          %%%
%%%   FOURIER TRANSFORM - Time to Frequency                                  %%%
%%%                                                                          %%%
%%%%%%%%%%%%%%%%%%%%%%%%%%%%%%%%%%%%%%%%%%%%%%%%%%%%%%%%%%%%%%%%%%%%%%%%%%%%%%%

Rft = fft(rt);
Rftnc = fft(rtnc);
Rf = fftshift(Rft);
Rfnc = fftshift(Rftnc);

%%%%%%%%%%%%%%%%%%%%%%%%%%%%%%%%%%%%%%%%%%%%%%%%%%%%%%%%%%%%%%%%%%%%%%%%%%%%%%%
%%%                                                                          %%%
%%%   LOW PASS FILTER                                                        %%%
%%%                                                                          %%%
%%%%%%%%%%%%%%%%%%%%%%%%%%%%%%%%%%%%%%%%%%%%%%%%%%%%%%%%%%%%%%%%%%%%%%%%%%%%%%%


Hlp = zeros(1,fz(2));

for i = 1:fz(2)
```

```
   if abs(f(i)) >= Bw
      Hlp(i) = 0;
  elseif (abs(f(i)) > f1) & (abs(f(i)) < Bw)
      Hlp(i) = (1/2) * (1 + cos(pi * (abs(f(i))-f1) / (2*fdelta)));
   else
      Hlp(i) = 1;
   end
end

Wout = Rf.*Hlp;
Woutnc = Rfnc.*Hlp;

Rfmag = abs(Rf)./max(abs(Rf));              % Scaling for plots
Rfpha = angle(Rf);                          % Scaling for plots
Rfmagnc = abs(Rfnc)./max(abs(Rfnc));        % Scaling for plots
Rfphanc = angle(Rfnc);                      % Scaling for plots
Womag = abs(Wout)./max(abs(Wout));          % Scaling for plots
Wopha = angle(Wout);                        % Scaling for plots
Womagnc = abs(Woutnc)./max(abs(Woutnc));    % Scaling for plots
Wophanc = angle(Woutnc);                    % Scaling for plots

o = o+1;
figure(o)
subplot(311)
plot(f,Rfmag)
ylabel('R(f)')
title('RX - BPSK Demodulated Spectrum')
axis([min(f)-0.05 max(f)+0.05 min(Rfmag) max(Rfmag)])
subplot(312)
plot(f,Hlp)
ylabel('G(f)')
title('RX - Low Pass Filter')
axis([min(f)-0.05 max(f)+0.05 min(Hlp) max(Hlp)])
subplot(313)
plot(f,Womag)
xlabel('Frequency (GHz)'), ylabel('Wout(f)')
title('RX - Output of Low Pass filter')
axis([min(f)-0.05 max(f)+0.05 min(Womag) max(Womag)])

%%%%%%%%%%%%%%%%%%%%%%%%%%%%%%%%%%%%%%%%%%%%%%%%%%%%%%%%%%%%%%%%%%%%%%%%%%%%%%%
%%%                                                                          %%%
%%%   INVERSE FOURIER TRANSFORM - Frequency to Time                          %%%
%%%                                                                          %%%
%%%%%%%%%%%%%%%%%%%%%%%%%%%%%%%%%%%%%%%%%%%%%%%%%%%%%%%%%%%%%%%%%%%%%%%%%%%%%%%

wouf = ifftshift(Wout);                % Shift spectrum
woufnc = ifftshift(Woutnc);            % Shift spectrum
wo = ifft(wouf);                       % Inverse Fourier Transform
wonc = ifft(woufnc);                   % Inverse Fourier Transform

%%%%%%%%%%%%%%%%%%%%%%%%%%%%%%%%%%%%%%%%%%%%%%%%%%%%%%%%%%%%%%%%%%%%%%%%%%%%%%%
%%%                                                                          %%%
%%%   SAMPLE and HOLD                                                        %%%
%%%                                                                          %%%
%%%%%%%%%%%%%%%%%%%%%%%%%%%%%%%%%%%%%%%%%%%%%%%%%%%%%%%%%%%%%%%%%%%%%%%%%%%%%%%

Vt = 0;                                % (V) Threshold voltage
tsym1 = tsym;
wout = zeros(1,nz(2)*tz(2));                % Initializes 'wout' vector
woutnc = zeros(1,nz(2)*tz(2));         % Initializes 'woutnc' vector

for j = 1:nz(2)
   t = j*Ts:dt:(j+1)*Ts-dt;            % Time vector for each symbol
```

```
   if mod(tz(2),2) == 0                % Parameter used for determining the
        a = tz(2)/2;                   % middle of the bit period and if the
   elseif mod(tz(2),2) == 1            % number of symbols is odd or even.
      a = (tz(2)-1)/2;
   end

   for i = 1:tz(2)                     % Sample and hold in the center of each bit
period
      if j == 1
         if i < a
            yt((j-1)*tz(2)+i) = 0;
            ytnc((j-1)*tz(2)+i) = 0;
         else
            yt((j-1)*tz(2)+i) = wo((j-1)*tz(2)+a);
            ytnc((j-1)*tz(2)+i) = wonc((j-1)*tz(2)+a);
         end
      elseif j < nz(2)
         if i < a
            yt((j-1)*tz(2)+i) = wo((j-2)*tz(2)+a);
            ytnc((j-1)*tz(2)+i) = wonc((j-2)*tz(2)+a);
         else
            yt((j-1)*tz(2)+i) = wo((j-1)*tz(2)+a);
            ytnc((j-1)*tz(2)+i) = wonc((j-1)*tz(2)+a);
         end
      else
         if i < a
            yt((j-1)*tz(2)+i) = wo((j-2)*tz(2)+a);
            ytnc((j-1)*tz(2)+i) = wonc((j-2)*tz(2)+a);
         else
            yt((j-1)*tz(2)+i) = 0;
            ytnc((j-1)*tz(2)+i) = 0;
         end
      end

      if (yt((j-1)*tz(2)+i) == Vt) & (j == 1) & (i < a)
         wout((j-1)*tz(2)+i) = 0;
      elseif yt((j-1)*tz(2)+i) > Vt    % Comparator
         wout((j-1)*tz(2)+i) = 1;
      else
         wout((j-1)*tz(2)+i) = -1;
      end

      if (ytnc((j-1)*tz(2)+i) == Vt) & (j == 1) & (i < a)
         woutnc((j-1)*tz(2)+i) = 0;
      elseif ytnc((j-1)*tz(2)+i) > Vt  % Comparator for non Atmosphere model
         woutnc((j-1)*tz(2)+i) = 1;
      else
         woutnc((j-1)*tz(2)+i) = -1;
      end
   end

   if j == 1
      tsym2 = t;
   else
      tsym2 = [tsym2 t];
   end
end

tsz = size(tsym1);

o = o+1;
figure(o)
```

```
subplot(411)
plot(tsym,real(rt),'m',tsym,real(wo),'k')
ylabel('r(t)')
title('RX - BPSK Demodulated Signal')
grid
axis([min(tsym)-2 max(tsym)+2 -1.2 1.2])
subplot(412)
plot(tsym,real(rtnc),'m',tsym,real(wonc),'k')
ylabel('r(t)')
title('RX - BPSK Demodulated Signal (NC)')
grid
axis([min(tsym)-2 max(tsym)+2 -1.2 1.2])
subplot(413)
plot(tsym,real(wo),'k')
ylabel('wo(t)')
title('RX - Filtered BPSK Demodulated Signal')
grid
axis([min(tsym)-2 max(tsym)+2 -1.2 1.2])
subplot(414)
plot(tsym,real(wonc),'k')
xlabel('Time (ps)'), ylabel('wo(t)')
title('RX - Filtered BPSK Demodulated Signal (NC)')
grid
axis([min(tsym)-2 max(tsym)+2 -1.2 1.2])

o = o+1;
figure(o)
subplot(311)
plot(tsym,mt,'b')
ylabel('m(t)')
title('TX - Digital Signal In')
axis([min(tsym2)-2 max(tsym2)+2 min(wout)-0.2 max(wout)+0.2])
subplot(312)
plot(tsym2,wout,'k')
ylabel('wout(t)')
title('RX - Output of Comparator')
axis([min(tsym2)-2 max(tsym2)+2 min(wout)-0.2 max(wout)+0.2])
subplot(313)
plot(tsym2,woutnc,'k')
xlabel('Time (ps)'), ylabel('wout(t)')
title('RX - Output of Comparator (NC)')
axis([min(tsym2)-2 max(tsym2)+2 min(wout)-0.2 max(wout)+0.2])

%%%%%%%%%%%%%%%%%%%%%%%%%%%%%%%%%%%%%%%%%%%%%%%%%%%%%%%%%%%%%%%%%%%%%%%%%%%%%%%
%%%                                                                          %%%
%%%   EYE DIAGRAM - Output Signal without oxygen present                         %%%
%%%                                                                          %%%
%%%%%%%%%%%%%%%%%%%%%%%%%%%%%%%%%%%%%%%%%%%%%%%%%%%%%%%%%%%%%%%%%%%%%%%%%%%%%%%

nt = 3;                                % Number of dt before and after the bit period
teye = 0 - nt*dt : dt : Ts + (nt-1)*dt;
vcnc = zeros(1,nz(2));

for j = 1:nz(2)
     teye2 = (j-1)*Ts - nt*dt : dt : j*Ts + (nt-1)*dt;
     tez = size(teye2);
     % T vector for the eye diagram

     for i = 1:tez(2)
          if j == 1
               if teye2(i) <= 0
                    etnc(j,i) = 0;
               elseif teye2(i) <= j*Ts-dt
```

```
                    etnc(j,i) = wonc((j-1)*tz(2)+(i-nt));
                    if teye2(i) == j*Ts/2
                         vcnc(1,j) = wonc((j-1)*tz(2)+(i-nt));
                    end
               else
                    etnc(j,i) = wonc((j-1)*tz(2)+(i-nt));
               end
          elseif j < nz(2)
               if teye2(i) <= (j-1)*Ts
                    etnc(j,i) = wonc((j-1)*tz(2)+(i-nt));
               elseif teye2(i) <= j*Ts-dt
                    etnc(j,i) = wonc((j-1)*tz(2)+(i-nt));
                    if teye2(i) == (j-1)*Ts+Ts/2
                         vcnc(1,j) = wonc((j-1)*tz(2)+(i-nt));
                    end
               else
                    etnc(j,i) = wonc((j-1)*tz(2)+(i-nt));
               end
          else
               if teye2(i) <= (j-1)*Ts
                    etnc(j,i) = wonc((j-1)*tz(2)+(i-nt));
               elseif teye2(i) <= j*Ts-dt
                    etnc(j,i) = wonc((j-1)*tz(2)+(i-nt));
                    if teye2(i) == (j-1)*Ts+Ts/2
                         vcnc(1,j) = wonc((j-1)*tz(2)+(i-nt));
                    end
               else
                    etnc(j,i) = 0;
               end
          end
     end

     eyenc(j,:) = etnc(j,:);

     if j == 1
         vpk1 = max(abs(real(etnc(j,:))));
     elseif j >= 2
          if vpk1 < max(abs(real(etnc(j,:))))
               vpk1 = max(abs(real(etnc(j,:))));
          end
     end

end

o = o+1;
figure(o)
hold on

for j = 1:nz(2)
     plot(teye, real(eyenc(j,:)));

end

titenc = ['Eye diagram without oxygen present in the link'];
xlabel('Time (ns)'), ylabel('wout(t) (V)')
title(titenc)
axis([(0 - (nt+3)*dt) (Ts + (nt-1+3)*dt) -0.5 0.5])
grid

hold off

%%%%%%%%%%%%%%%%%%%%%%%%%%%%%%%%%%%%%%%%%%%%%%%%%%%%%%%%%%%%%%%%%%%%%%%%%%%%%%
%%%                                                                        %%%
```

```
%%%   EYE DIAGRAM - Output Signal with oxygen present                    %%%
%%%                                                                     %%%
%%%%%%%%%%%%%%%%%%%%%%%%%%%%%%%%%%%%%%%%%%%%%%%%%%%%%%%%%%%%%%%%%%%%%%%%%%%%

vc = zeros(1,nz(2));


for j = 1:nz(2)
     teye2 = (j-1)*Ts - nt*dt : dt : j*Ts + (nt-1)*dt;
     tez = size(teye2);
     % T vector for the eye diagram

     for i = 1:tez(2)
          if j == 1
               if teye2(i) <= 0
              et(j,i) = 0;
               elseif teye2(i) <= j*Ts-dt
                    et(j,i) = wo((j-1)*tz(2)+(i-nt));
                    if teye2(i) == j*Ts/2
                         vc(1,j) = wo((j-1)*tz(2)+(i-nt));
                    end
               else
                    et(j,i) = wo((j-1)*tz(2)+(i-nt));
               end
          elseif j < nz(2)
               if teye2(i) <= (j-1)*Ts
                    et(j,i) = wo((j-1)*tz(2)+(i-nt));
               elseif teye2(i) <= j*Ts-dt
                    et(j,i) = wo((j-1)*tz(2)+(i-nt));
                    if teye2(i) == (j-1)*Ts+Ts/2
                         vc(1,j) = wo((j-1)*tz(2)+(i-nt));
                    end
               else
                    et(j,i) = wo((j-1)*tz(2)+(i-nt));
               end
          else
               if teye2(i) <= (j-1)*Ts
                    et(j,i) = wo((j-1)*tz(2)+(i-nt));
               elseif teye2(i) <= j*Ts-dt
                    et(j,i) = wo((j-1)*tz(2)+(i-nt));
                    if teye2(i) == (j-1)*Ts+Ts/2
                         vc(1,j) = wo((j-1)*tz(2)+(i-nt));
                    end
               else
                    et(j,i) = 0;
               end
          end
     end

     if j == 1
          vpk2 = max(abs(real(et(j,:))));
     elseif j >= 2
          if vpk2 < max(abs(real(et(j,:))))
               vpk2 = max(abs(real(et(j,:))));
          end
     end

     eyec(j,:) = et(j,:);
end

o = o+1;
figure(o)
hold on
```

```
for j = 1:nz(2)
     Vc(1,j) = vc(1,j)*vpk1/vpk2;
     eyecn(j,:) = eyec(j,:)*vpk1/vpk2;
     plot(teye, real(eyecn(j,:)));

end


tite = ['Eye diagram with oxygen present in the link with P = ' Pres ' mbar and dist =
' Dist ' km'];
xlabel('Time (ns)'), ylabel('wout(t) (V)')
title(tite)
axis([(0 - (nt+3)*dt) (Ts + (nt-1+3)*dt) -0.5 0.5])
grid

hold off
```

Table A.1 - Parameters for Local Line Contribution.

a_1 (kHz/mbar)	a_2	a_3 (GHz/mbar)	a_4	a_5 ($mbar^{-1}$)	a_6 ($mbar^{-1}$)	f_o (GHz)
0.9400	9.694	8.60	0	1.600	5.520	50.474238
2.460	8.694	8.70	0	1.400	5.520	50.987749
6.080	7.744	8.90	0	1.165	5.520	51.503350
14.14	6.844	9.20	0	0.883	5.520	52.021410
31.02	6.004	9.40	0	0.579	5.520	52.542394
64.10	5.224	9.70	0	0.252	5.520	53.066907
124.7	4.484	10.00	0	-0.066	5.520	53.595749
228.0	3.814	10.20	0	-0.314	5.520	54.130000
391.8	3.194	10.50	0	-0.706	5.520	54.671159
631.6	2.624	10.79	0	-1.151	5.514	55.221367
953.5	2.119	11.10	0	-0.920	5.025	55.783802
548.9	0.015	16.46	0	2.881	-0.069	56.264775
1344.0	1.660	11.44	0	-0.596	4.750	56.363389
1763.0	1.260	11.81	0	-0.556	4.104	56.968206
2141.0	0.915	12.21	0	-2.414	3.536	57.612484
2386.0	0.626	12.66	0	-2.635	2.686	58.323877
1457.0	0.084	14.49	0	6.848	-0.647	58.446590
2404.0	0.391	13.19	0	-6.032	1.858	59.164207
2112.0	0.212	13.60	0	8.266	-1.413	59.590983
2124.0	0.212	13.82	0	-7.170	0.916	60.306061
2461.0	0.391	12.97	0	5.664	-2.323	60.434776
2504.0	0.626	12.48	0	1.731	-3.039	61.150560
2298.0	0.915	12.07	0	1.738	-3.797	61.800154
1933.0	1.260	11.71	0	-0.048	-4.277	62.411215
1517.0	0.083	14.68	0	-4.290	0.238	62.486260
1503.0	1.665	11.39	0	0.134	-4.860	62.997977
1087.0	2.115	11.08	0	0.541	-5.079	63.568518
733.5	2.620	10.78	0	0.814	-5.525	64.127767
463.5	3.195	10.50	0	0.415	-5.520	64.678903
274.8	3.815	10.20	0	0.069	-5.520	65.224071
153.0	4.485	10.00	0	-0.143	-5.520	65.764772
80.09	5.225	9.70	0	-0.428	-5.520	66.302091
39.46	6.005	9.40	0	-0.726	-5.520	66.836830
18.32	6.845	9.20	0	-1.002	-5.520	67.369598
8.010	7.745	8.90	0	-1.255	-5.520	67.900867
3.300	8.695	8.70	0	-1.500	-5.520	68.431005
1.280	9.695	8.60	0	-1.700	-5.520	68.960311

References

1 H. J. Liebe. "MPM – An Atmospheric Millimeter-wave Propagation Model." International Journal of Infrared and Millimeter Waves. 10.6 (1989): 631-650.

2 J. E. Allnutt. Satellite-to-Ground Radiowave Propagation: Theory, Practice and System Impact at Frequencies above 1 GHz. London: Peter Peregrinus Ltd., 1989.

3 Federal Communications Commission. "Use of Radio Frequencies Above 40 GHz for New Radio Applications." FCC 94-273. November 30, 1994. <http://www.fcc.gov/Bureaus/Engineering_Technology/Documents/fedreg/59/61304.txt>

4 Federal Communications Commission. Code of Federal Regulations. 47CFR15.255. October 1, 2000.

5 F. Giannetti, M. Luise, and R. Reggianni. "Mobile and Personal Communications in the 60 GHz Band: A Survey." Wireless Personal Communications. 10 (1999): 207-43.

6 M. Luise and S. Pupolin (eds.). Broadband Wireless Communications. Springer-Verlag: London, 1998.

7 A. Plattner, "Technology and Demonstrator of the RACE Project 'Mobile Broadband System'." In the *IEEE MTT-S International Microwave Symposium*. San Diego, CA. 1994.

8 L. Fernandes. "R2067 MBS – Mobile Broadband System." In the *2nd IEEE International Conference on Universal and Personal Communications*. Ottawa. 1993

9 CORDIS RTD-PROJECTS/© European Communities. "Wireless Broadband CPN LAN for Professional and Residential Multimedia Applications." Project MEDIAN, ACTS AC006. March, 1998. <http://dbs.cordis.lu/cordis-cgi/srchidadb?ACTION=D&SESSION=154662001-6-4&DOC=49&TBL= EN_PROJ&RCN=EP_RCN:30450&CALLER=EN_UNIFIEDSRCH>.

10 CORDIS RTD-PROJECTS/© European Communities. "System for Advanced Mobile Broadband Applications." Project SAMBA, ACTS AC204. November 1996. <http://dbs.cordis.lu/cordis-cgi/srchidadb?ACTION=D&SESSION=156272001-6-4&DOC=1&TBL=EN_ACRO&RCN=EA_RCN: 7909&CALLER=EN_CORDIS>.

11 L.J. Greestein, et. al. "Microcells in Personal Communications Systems." IEEE Communications Magazine. (1992): 76-88.

12 D. Molkdar. "Review on Radio Propagation into and within Buildings." IEE Proceedings, Part H. (1991): 943-967.

13 H. Hashemi. "The Indoor Radio Propagation Channel." In the *Proceedings of the IEEE*. (1993): 943-967.

14 J.B. Andersen, T.S. Rappaport and S. Yoshida. "Propagation Measurements and Models for Wireless Communications Channels." IEEE Communications Magazine. (1995):42-49.

15 R. Steele and V.K. Prabhu. "High-User Density Digital Cellular Mobile Radio Systems." IEE Proceedings, Part F. (1985): 396-404.

16 R.K. Jurgen. "Smart Cars and Highways Go Global." IEEE Spectrum. (1991): 26-36.

17 J.P. Altendorf, et. al. "An Assessment Scheme for Transmission Systems Applied to Road Transport Telematics." In the Proceedings of the *SAE Future Transportation Technology Conference and Display*. San Diego, CA. 1990.

18 R. Steele (ed.). Mobile Radio Communications. London: Pentech Press, 1992.

19 H. Meinel, A. Plattner and G. Reinhold. "A 40 GHz Railway Communication System." IEEE Journal on Selected Areas in Communications. (1983): 615-22.

20 H. Meinel and A. Plattner. "Millimeter-Wave Propagation Along Railway Lines." IEE Proceedings, Part F. (1983): 688-94.

21 T.S. Perry and L. Geppert. "Do Portable Electronics Endanger Flight?" IEEE Spectrum. (1996): 26-33.

22 R. Steele. "Towards a High-Capacity Digital Cellular Mobile Radio System." IEE Proceedings, Part F. (1985): 405-15

23 E. Damosso, L. Stola and G. Brussard. "Characteristics of the 50-70 GHz Band for Space Communications." ESA Journal. 7. (1983): 25-43

24 G. Anzic, et. al. "A Study of 60 GHz Intersatellite Link Application." In the Proceedings of *IEEE ICC*. Boston, MA. 1983.

25 H. Meinel. "Millimeter Wave System Design and Application Trends in Europe." Alta Frequenza. (1989): 441-56

26 P.M. Brigginshaw and A.S. Restarick. "60 GHz Covert Communication Link in Binocular." In the Proceedings of the *Military Microwave Conference*. Brighton. 1986.

27 ULTRA FAST SYSTEMS. "Microwave and Millimetre-Wave Applications." <http://www.elec.gla.ac.uk/groups/nano/UFS/apps.html>.

28 Harmonix Corporation. "GigaLink Overview." <http://www.hxi.com/overview.html>

29 Harmonix Corporation. "GigaLink Features." <http://www.hxi.com/features.html>

30 J. H. Van Vleck. "The Absorption of Microwaves by Oxygen." Physical Review. 71.7 (1947): 413-24.

31 H. G. Kuhn. Atomic Spectra. New York: Academic Press: 1969.

32 J. H. Van Vleck and V. F. Weisskopf. "On the Shape of Collision-Broadened Lines." Reviews of Modern Physics. 17.2-3 (1945): 227-36.

33 H. J. Liebe, P. W. Rosenkranz, and G. A. Hufford. "Atmospheric 60-GHz Oxygen Spectrum: New Laboratory Measurements and Line Parameters." Journal of Quantitative Spectroscopy & Radiative Transfer. 48.5-6 (Nov.-Dec. 1992): 629-43.

34 G. Brussard and P.A. Watson. Atmospheric Modeling and Millimetre Wave Propagation. London: Chapman & Hall, 1995.

35 H. J. Liebe. "Modeling Attenuation and Phase of Radio Waves in Air at Frequencies below 1000 GHz." Radio Science. 16.6 (1981): 1183-99.

36 H. J. Liebe, G. A. Hufford, and M. G. Cotton. "Propagation Modeling of Moist Air and Suspended Water/Ice Particles at Frequencies Below 1000 GHz." In the Conference Proceedings of AGARD meeting on '*Atmospheric Propagation Effects through Natural and Man-Made Obscurants for Visible to MM-Wave Radiation' (AGARD-CP-542).* Neuilly sur Seine, France. May 1993.

37 H. J. Liebe. "An Updated Model for Millimeter Wave Propagation in Moist Air." Radio Science. 20.5 (1985): 1069-1089.

38 P. W. Rosenkranz. "Shape of the 5 mm Oxygen Band in the Atmosphere." IEEE Transactions on Antennas and Propagation. 23.4 (1975): 498-506.

39 P. W. Rosenkranz. "Interference Coefficients for Overlapping Oxygen Lines in Air." Journal of Quantitative Spectroscopy & Radiative Transfer. 39.4 (1988): 287-297.

40 H. J. Liebe and G. A. Hufford. "Modeling Millimeter-wave Propagation Effects in the Atmosphere." In the Conference Proceedings of AGARD meeting on '*Atmospheric Propagation in the UV, Visible, IR and MM-Wave Region and Related Systems Aspects' (AGARD-CP-454).* Neuilly sur Seine, France. October 1989.

41 L. W. Couch. Digital and Analog Communication Systems. 6th ed. New Jersey: Prentice Hall, 2001.

42 T. Pratt. "8. Digital Transmission Systems." 4644 Lecture Notes. Spring 2001

43 United States. Committee on Extension to the Standard Atmosphere. U.S. Standard Atmosphere, 1976. Washington: GPO, 1976.